Journal of Volcanology and Geothermal Research 440 (2023) 107846

Contents lists available at ScienceDirect

Journal of Volcanology and Geothermal Research

journal homepage: www.journals.elsevier.com/journal-of-volcanology-and-geothermal-research

The spatial and volcanic evolution of Ayelu, Abida and Yangudi volcanoes in the Northern Main Ethiopian Rift – Southern Afar, Ethiopia

Rhiannon Rees [a,*], Thomas M. Gernon [a], Derek Keir [a,b], Rex N. Taylor [a], Carolina Pagli [c]

[a] School of Ocean and Earth Science, University of Southampton, European Way, Southampton SO14 3ZH, UK
[b] Dipartimento di Scienze della Terra, Università degli Studi di Firenze, Firenze 50121, Italy
[c] Dipartimento di Scienze della Terra, Università di Pisa, Via S. Maria 53, Pisa 56126, Italy

ARTICLE INFO

Keywords:
Afar
Main Ethiopian Rift
Adda'do Magmatic Segment (AMS)
Continental rifting
Bimodal volcanism

ABSTRACT

The region between the Northern Main Ethiopian Rift and Southern Afar is a key link between two important sectors of the East African Rift System. Recent volcanism in this area occurs as a chain of NNE-SSW trending axial Quaternary volcanoes and volcanic fields, segmented and offset laterally by WNW-ESE trending right-steps. Here, we present the first whole-rock major element geochemical dataset from volcanoes in one such volcanic segment, the Adda'do Magmatic Segment (AMS). We combine these geochemical data with detailed remote sensing mapping of the region, to produce a relative chronology of the volcanic units. We investigate the volcanic evolution and composition of these volcanoes and find that all three volcanoes in the AMS exhibit similar evolutionary patterns, beginning with a base of older (presumed Plio-Pleistocene age) lavas, followed by a period of large-volume evolved magmatism, and recent basaltic-intermediate eruptions. Our results show evidence for at least three cycles of mafic-to-felsic evolution in the southern AMS, in agreement with earlier studies, indicating that the AMS has long been a site of volcanic activity.

1. Introduction

The East African Rift System (EARS) is the world's longest and best exposed example of a continental rift, and thus presents an ideal location to study the magmatic expression of active rift systems. Varying stages of rift development are manifested along the EARS, from early-stage continental rifting in the southern Malawi Rift, to near continental breakup in the Danakil region of Afar (Ebinger, 2005; Corti, 2009). Despite its geological importance as a region of contrasting rifting styles and progressive rift sector development, large sections of the EARS remain understudied – including where the Northern Main Ethiopian Rift links with the Red Sea and Gulf of Aden in Southern Afar (Chernet et al., 1998). In Southern Afar, there is a significant gap in understanding of volcano evolution, as well as a paucity of geochemical and chronological data which limits our understanding of controls on magmatic system evolution during rift evolution. As a result, we lack understanding of a number of broader scale questions on mantle melt zone variability, variations in characteristics of magma plumbing systems with rift evolution, and also local understanding of volcanic histories and hazards in these regions.

Here, we focus on the Adda'do Magmatic Segment (AMS), the largest and most active area of volcanic activity in Southern Afar (Fig. 1). The AMS comprises three volcanoes – Yangudi (also spelled Angudi, Jangudi), Ayelu (also spelled Agelu, Ayalu, Aielu) and Abida (also known as Adwa, Aabida, Amoissa and Dabita) – at least one of which is thought to have actively erupted in the last few hundred years (Global Volcanism Program, 2013). In this paper, we use remote sensing techniques to produce a detailed, updated relative chronology for erupted units at Ayelu, Abida and Yangudi. This age model is used in conjunction with whole rock major element data from 45 rock samples to provide the first detailed study of the volcanic and geochemical evolution of Ayelu, Abida and Yangudi. Our new analyses place fundamental constraints on the composition and relative chronology of deposits erupted from these volcanoes providing a framework for future work in this area.

2. Geological background

2.1. Northern Main Ethiopian Rift and Southern Afar

Afar is located on the junction of three rifts, the Red Sea Rift to the northwest, the Gulf of Aden Rift to the northeast, and the Main Ethiopian Rift (MER) to the south (Fig. 1). Together, Afar and the MER form the

* Corresponding author.
E-mail address: r.rees@soton.ac.uk (R. Rees).

https://doi.org/10.1016/j.jvolgeores.2023.107846
Received 9 March 2023; Received in revised form 14 June 2023; Accepted 16 June 2023
Available online 17 June 2023

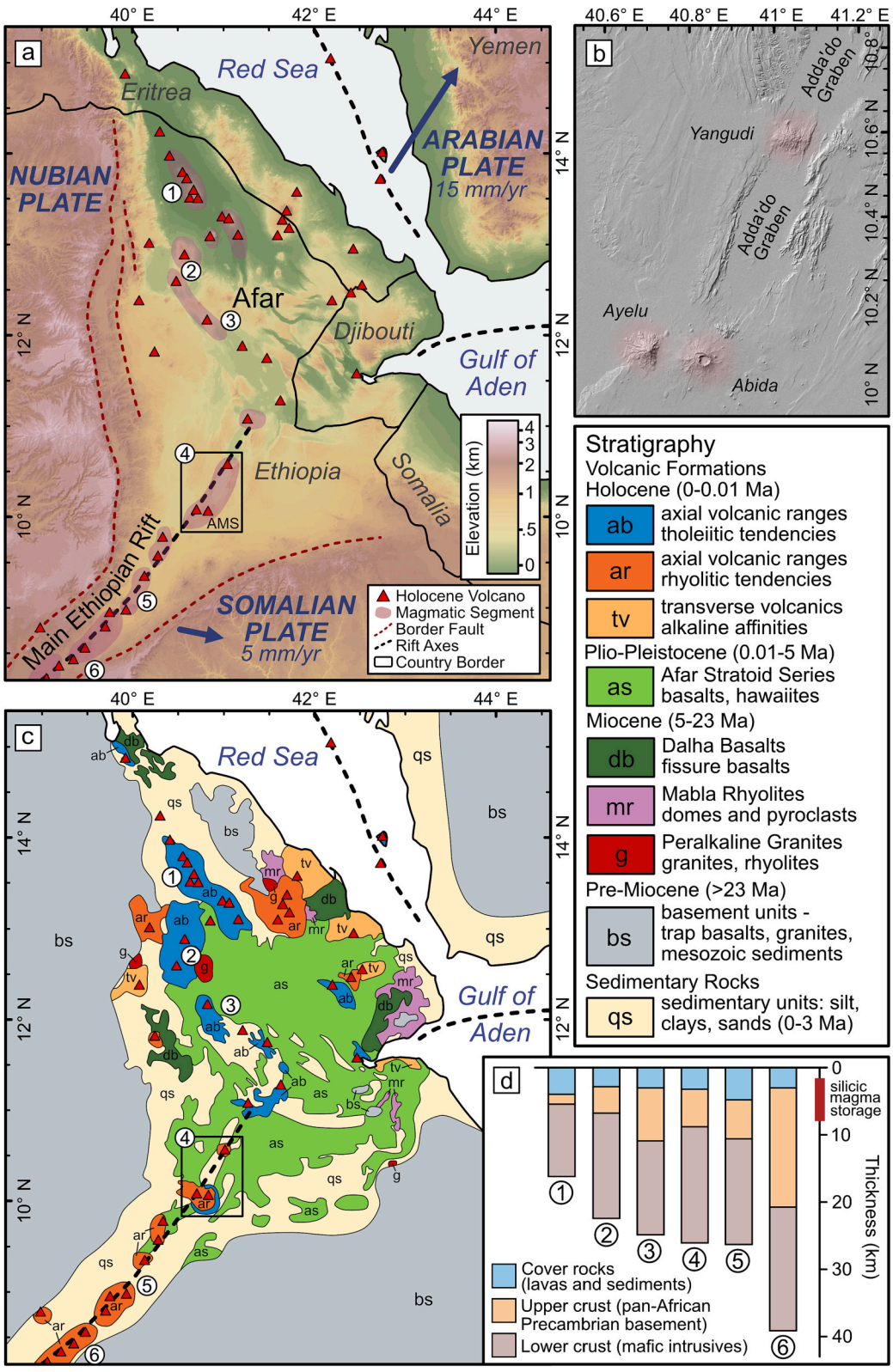

Fig. 1. (a) Topographic map of Afar and the NMER. Arrows show generalised extension rates and directions of the Arabian and Somalian Plates relative to a fixed Nubian Plate (McClusky et al., 2010; Saria et al., 2014). Elevation data from NASA SRTM, Holocene volcano location data from the Smithsonian Institution Global Volcanism Program, magmatic segments and fault locations mapped in agreement with literature (e.g. Chorowicz, 2005; Keir et al., 2011). (b) hillshaded relief map of the Adda'do Magmatic Segment (AMS) showing the three volcanoes Abida, Ayelu and Yangudi. (c) generalised geological map and stratigraphic column of Afar and the NMER (after Varet, 1975; Beyene and Abdelsalam, 2005). (d) Summary of crustal thickness and composition for six locations in the MER/Afar, marked as numbered circles on maps (a) and (b) (location 1 = Erta Ale Segment, locations 2, 3 = Manda Hararo Rift Segment, location 4 = Adda'do Magmatic Segment, location 5 = Boset, Northern Main Ethiopian Rift, location 6 = Aluto, Main Ethiopian Rift. Crustal compositions and thickness are derived from active-source seismic experiments and receiver function studies (Hammond et al., 2011; Hutchison et al., 2018). Approximate depths of silicic magma reservoirs are based on deformation, seismic and petrological constraints (Hutchison et al., 2018 – and references therein).

most northerly sections of the East African Rift System (EARS), a tectonically- and volcanically-active continental rift system that stretches nearly 3000 km down the eastern portion of Africa. Rifting began in the Red Sea and Gulf of Aden at c. 26–29 Ma and 35 Ma respectively (Wolfenden et al., 2005; Ayalew et al., 2006; Leroy et al., 2010; Zwaan et al., 2020). By comparison, initial rifting in the MER is believed to have begun as late as 11 Ma in the Northern Main Ethiopian Rift (NMER) (Wolfenden et al., 2004).

Southernmost Afar, the region between Afar and the MER (sometimes known as the Northern Main Ethiopian Rift – Southern Afar Transition Zone, e.g. Chernet et al., 1998; Chernet and Hart, 1999) is an important physiographic, structural, tectonic and volcanological link between these two portions of the EARS (Chernet and Hart, 1999). The early stages (c. 29–11 Ma) of the development of Southern Afar were controlled by opening of the Red Sea and Gulf of Aden.

By contrast, since the development of the MER and formation of a triple junction at ~11 Ma (Wolfenden et al., 2004), this region is characterised structurally and volcanically as being the northernmost expression of the MER. The extension in the MER has localised through time and is currently mainly focused in the Wonji Fault Belt (WFB), a 10–20 km wide zone of normal faulting and volcanism relating to Quaternary extension (Mohr and Wood, 1976; Siegburg et al., 2020). The WFB comprises six NNE trending magmatic segments, offset laterally from each other by 10–40 km in a right-stepping fashion (Fig. 2) (Ebinger and Hayward, 1996; Chernet and Hart, 1999). Consequently, Southern Afar shares tectonic history and rheological properties with both Central Afar to the north and the MER to the south (Tesfaye et al., 2003).

Volcanism in the NMER – Southern Afar began at around 30 Myr before the onset of any significant extension, with the eruption of Afar plume-related flood basalts (Fig. 1c; unit 'bs') (Ebinger et al., 1993; Pik et al., 1998; Stab et al., 2016; Hofmann et al., 1997). $^{40}Ar/^{39}Ar$ dating suggests that the majority of these Ethiopian flood basalts were erupted rapidly (within one million years) at around 30 Ma (Hofmann et al., 1997; Chorowicz, 2005). A second wave of flood basalt eruptions, known as the Afar Stratoid Series, began in Afar at around 4.4 Ma and ended at around 500,000 years ago, with peak activity occurring around 2 Ma (Fig. 1c; unit 'as') (Ebinger et al., 1993; Chernet et al., 1998; Wolfenden et al., 2004; Stab et al., 2016; Tortelli et al., 2022). The Afar Stratoid flood basalt eruptions were so extensive they cover up to 70% of the modern-day rift floor surface in Afar (Varet, 2017).

Quaternary rift volcanism in the NMER and Southern Afar consists predominantly of bimodal basalt-rhyolite volcanism (Gasparon et al., 1993; Trua et al., 1999), which began developing in Southern Afar during the late Miocene at around 7 Ma (Fig. 1c; units 'ab', 'ar' and 'tv') (Chernet et al., 1998). This recent volcanism consists of regularly spaced (43 ± 13 km; Mohr and Wood, 1976) predominantly silicic on-axis volcano complexes, with volcanic fields of mainly mafic composition (Mohr and Wood, 1976; Rooney et al., 2005; Fontijn et al., 2018; Rooney, 2020a). The main volcanic centres, from south to north, are Corbetti, Aluto, Gedemsa, Boset-Bericha Volcanic Complex (BBVC), Kone, Fantale, Dofan, Ayelu and Abida, Yangudi, Gabillema, and Dama Ali (Fig. 2). The northernmost of these volcanoes (from Dofan to Dama Ali) are usually considered to be part of Southern Afar, whilst the remaining southerly volcanoes are considered to be part of the MER (e.g. Chernet and Hart, 1999; Fontijn et al., 2018).

2.2. The Adda'do Magmatic Segment (AMS)

The Adda'do Graben is the youngest and most tectonically active

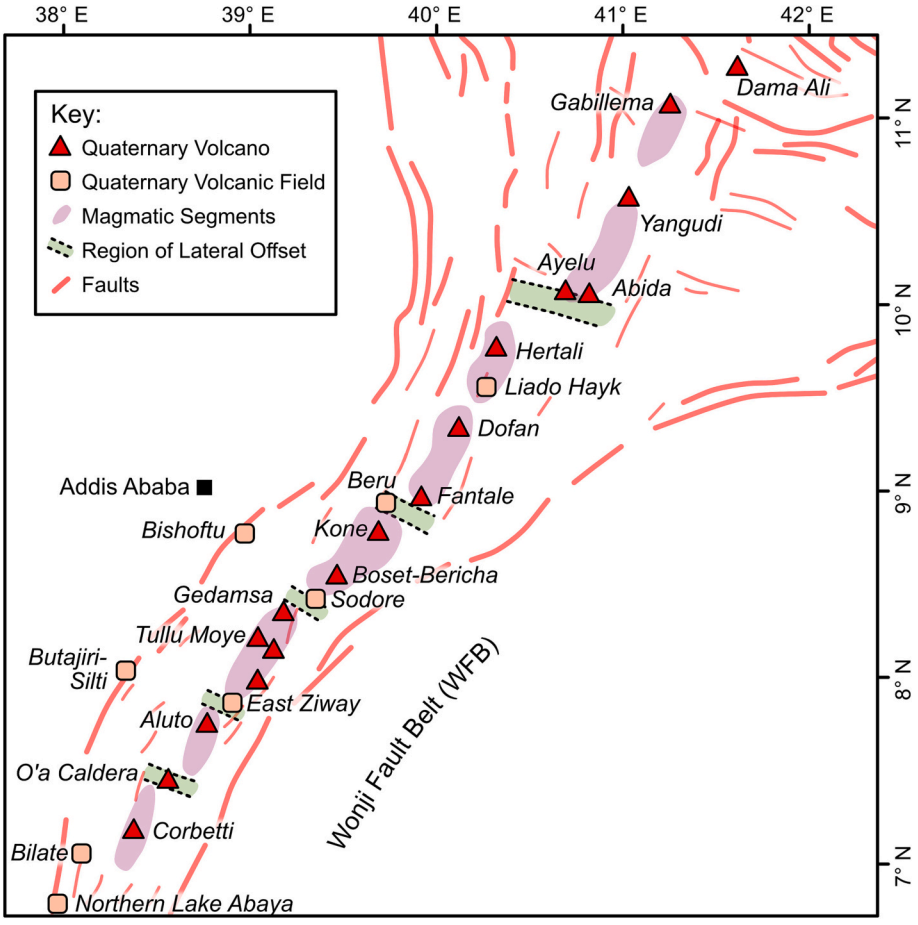

Fig. 2. Schematic map of the main Quaternary volcanoes (predominantly stratovolcanoes and volcanic complexes, usually with some evolved components), volcanic fields (areas of localised volcanic activity consisting of clusters of cinder cones and/or lava flows), and major magmatic and tectonic features of Southern Afar – Main Ethiopian Rift, after Chernet et al. (1998). The Wonji Fault Belt (WFB) refers to the 10–20 km wide zone of normal faulting within the magmatic segments along the rift floor in Northern Afar/Southern MER (Mohr and Wood, 1976; Siegburg et al., 2020). There are six main NNE trending magmatic segments in the MER. Magmatic segment locations and fault locations after Corti et al. (2015), Ebinger and Hayward (1996) and Wright et al. (2012); locations and categorisation of volcanoes and volcanic fields from Global Volcanism Program (2013).

graben in Southern Afar (Varet, 2017). This 20 km-wide graben marks the junction between the Main Ethiopian Rift and Southern Afar, and is volcanically active, with the stratovolcanoes Ayelu and Abida in the south and Gabillema in the north (Fig. 2). The stratovolcano Yangudi bisects the Adda'do Graben, and together these three most southerly volcanoes (Ayelu, Abida and Yangudi) collectively form the Adda'do Magmatic Segment (AMS) (Fig. 2). Formerly, Gabillema was referred to as being part of the AMS, however now it is generally considered its own distinct magmatic segment (Casey et al., 2006; Rooney, 2020a) (Fig. 2).

Within the AMS, the volcanoes Ayelu and Abida are situated on a WNW-ESE trending region of rift lateral offset at the end of the magmatic segment, whereas Yangudi is located within the axial centre of the rift (Fig. 2). Previous studies of the AMS volcanoes are limited, with very little geochemical data available (Ayalew et al., 2016; Rooney, 2020a). Age data too are very limited, with only one age determination from Ayelu (500 ka for lavas sampled at the base of Ayelu; Varet, 2017) and no ages for the other two volcanoes.

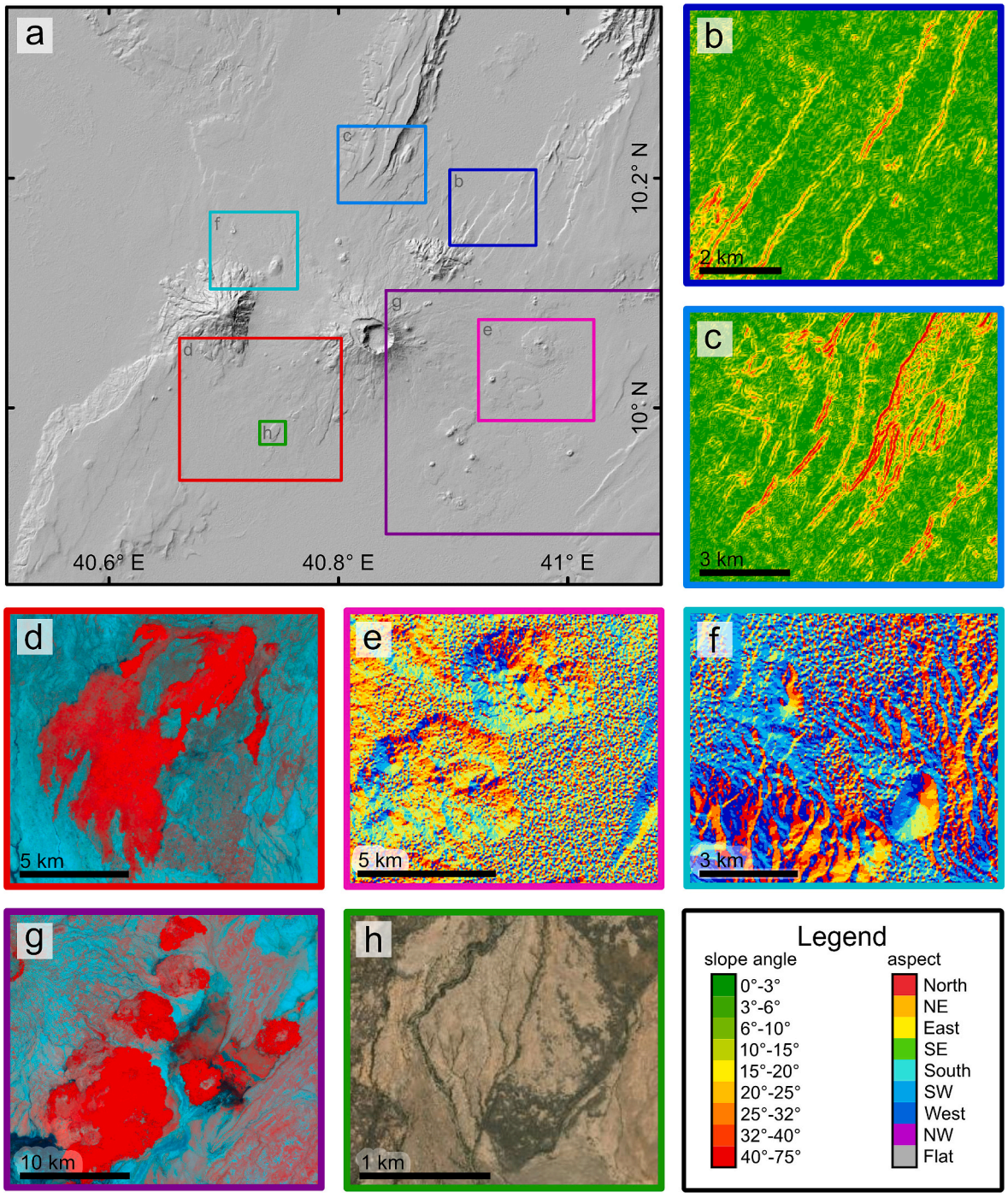

Fig. 3. Examples of the datasets and tools used in ArcMap 10.5 to map structural and geological features in the study area. (a) Hillshaded elevation model derived from SRTM DEM; (b) and (c) slope angle (spatial analyst) derived from SRTM DEM; (d) and (g) false-colour multispectral band ratio satellite images derived from Landsat 8 images (5/4, 5/1 and 3/7 in RGB respectively); (e) and (f) slope aspect (spatial analyst) derived from SRTM DEM; (h) true colour satellite imagery (CNES/ Airbus DS; Landsat/Copernicus; Maxar Technologies). Labelled/colour coded boxes in (a) mark the geographic locations of sites (b) to (h).

3. Methodology

3.1. Remote sensing mapping and geochronology

Volcanic and geological features of Ayelu, Abida and Yangudi were mapped in ArcMap 10.5 (UTM WGS 1984 Zone 37 N) using remote sensing data. Multispectral Landsat 8 imagery (spatial resolution 30 m) and panchromatic satellite imagery (CNES/Airbus DS; Landsat/Copernicus; Maxar Technologies, spatial resolution up to 1 m) along with a digital elevation model (NASA SRTM, spatial resolution 30 m) were used with morphometric and topographic functions in ArcMap 10.5 to help identify volcanic features such as distinct geological units, individual lava flows and cones, and structural features such as faults and fractures.

Sensitive to subtle changes in topography, the slope, aspect and hillshade spatial analyst tools (input raster: NASA SRTM DEM) were used to identify lava and tuff deposits and tectonic features and to map the cross-cutting relationships between these features (Fig. 3). Multispectral Landsat 8 imagery was used in the band ratio combinations 5/4, 5/1 and 3/7 in RGB respectively to highlight deposits of mafic composition (Patel and Solanki, 2020). 3D visualisations in Google Earth Pro were also used to help identify cross cutting relationships between defined units, to develop a relative age model of the area. Where possible, maximum volume estimates for individual flows and units (Sections 4.1.1 and 4.1.2) were calculated using the surface area of the flow/unit as drawn in ArcMap, multiplied by the estimated average thickness of the flow/unit above the background baseline. This thickness was estimated by drawing a series of topographic profiles across the flow/unit using NASA SRTM DEM height data.

These data and spatial analyst tools were used in conjunction with the 1975 publication "Carte géologique de l'Afar central et meridional" (geological map of central and southern Afar) (Varet, 1975). This map shows the main stratigraphic, volcanic and sedimentary units and structural features for southern Afar, from 10°N (Ayelu/Abida) to 13°N. Modern satellite imagery and DEMs have allowed us to map the three volcanoes in more detail than was possible in 1975. Age estimates were assigned to the units we mapped by correlating them to those ages shown on the geological map published by Varet (1975) – where one absolute age of around 500 ka (mid-Pleistocene) has been determined from lava samples at the base of Ayelu. The remaining units at Ayelu, and all the units at Abida and Yangudi were assigned relative ages derived from cross-cutting relationships (see above), as no absolute ages exist for these volcanoes. Chemical compositions for volcanic units were determined through the whole-rock major element analysis of 45 rock samples (this study, see Section 4.2.). Where no rock sample was available for analysis, compositions were determined either from correlation with "Carte géologique de l'Afar central et meridional" (Varet, 1975), or from remote sensing observations of known units with similar appearances.

3.2. Major element geochemical analyses

A total of 45 rock samples (34 lavas and 11 tuffs) from the Afar Repository collection at the University of Pisa were chosen for major element analysis (sample locations in decimal degrees latitude/longidtude are given in Table 1, and sample locations are plotted on maps shown in Figs. 5 and 6). These samples were collected during several French-Italtian expeditions to Afar in the 1970s. To our knowledge, no prior geochemical work has been done on these rock samples. The samples were crushed and sorted into size fractions using a three-tier Teflon sieve set. The middle fraction samples (rock chips 0.5 mm to 1 mm) were cleaned by ultrasonicating and rinsing in MQ water to remove powder and dust. Samples were then dried at 85 °C for 12 h and were handpicked under a microscope to remove weathered grains and non-rock material. The cleaned rock chips were then manually ground to a fine powder using an agate mortar and pestle, to eliminate contamination that could occur using a porcelain or metal grinder. For major element analysis by XRF, first loss on ignition (LOI) for each sample was determined by weighing the samples before and after heating them to 950 °C for 3 h. Glass discs for major element analysis were prepared in platinum vials on the Vulcan Gas-Oxygen Fusion Bead Maker at the University of Southampton, using 0.5 g ignited sample powder with 5 g lithium tetraborate flux (exact ratio 1:10). Whole rock major element analyses of the fusion beads were then undertaken for a pilot 13 samples on the Philips MagiX Pro Xray fluorescence spectrometer at the University of Southampton, and on a Panalytical Axios XRF spectrometer at the Geological Survey of Japan/AIST for the remaining 32 samples. Analytical standards and accuracy were monitored using international standards JB-3, BCR-2, BIR-1 and SDC-1, and the internal standard BRR-1 (Supplementary Data 1).

3.3. Petrography

Petrographic observations of 41 thin section samples from the Afar Repository collection at the University of Pisa were gathered using a Meiji MT9300 petrographic microscope. For each thin section, total percentage areas of groundmass, vesicles, and major phenocryst phases were estimated, and textural observations were recorded. The majority of these thin section samples correspond to the rock samples used in the geochemical analyses (see the Supplementary Material for further details).

4. Results

4.1. Geological map of the AMS volcanoes – a relative geochronology

Using the combination of remote sensing techniques described above, we present a new geological map for Yangudi, Abida and Ayelu (Figs. 4 to 6). Major volcanic units and lava flows, along with the locations of major faults, satellite cones, and location and composition of rock samples are shown. A relative chronology of volcanic units has been established using cross-cutting relationships in 2D imagery and in 3D models, in conjunction with published age data from Varet (1975).

Here, we describe the geology of Ayelu and Abida together due to their proximity and physical overlap of deposits, and Yangudi separately due to its spatial and tectonic separation from the other two volcanoes. We describe the main volcanic units for all volcanoes from oldest to youngest.

4.1.1. Volcanic evolution of Ayelu and Abida

Stage 1: Plio-Pleistocene rift floor basalts. Pre-dating the main volcano building eruptions, the rift floor basalts at Ayelu and Abida are now only visible at two outcrops, one to the southwest and one to the northeast of Abida. The rift floor basalts are mid-brown in colour and have a blocky a'a texture. In contrast to younger lava flows at Abida and Ayelu, much of this unit has been obscured by a significant covering of recent Quaternary sediments (desert sands and silts), which makes the mapping of any individual flows or features within this unit difficult. These outcrops are dotted with numerous small volcanic cones (up to 250 m diameter and 15 m high), which in the southwest run in a general SSW-NNE trend, approximately parallel to the rift axis (Fig. 4). The source of these rift floor basalts is assumed to be rift fissures, now likely obscured by the main bulk of the Ayelu and Abida volcanoes and recent Quaternary sediment cover. It is likely that this rift floor basalt phase is far more extensive than can be seen now, due to subsequent sedimentation and covering by subsequent lava flows and tuff deposits.

Stage 2: Holocene volcanism. Holocene volcanism at Ayelu and Abida is dominated by felsic volcanism, both in the form of tuff deposits as well as significant felsic lava flows. On Abida, some intermediate and basaltic lava flows occur, particularly to the north and northwest of the main summit of the volcano.

The tuff deposits erupted from Abida blanket a large area, in some cases as far as 30 km from the summit. They cover most of the southern

Table 1
XRF major element data for all 45 samples analysed. Location information is provided in decimal degrees. All concentrations are reported as wt%, rock types have been allocated based on the TAS classification diagram in Fig. 7. Standards and errors associated with the XRF measurements are given in supplementary data (SD1).

Sample	Volcano	Latitude (°N)	Longitude (°E)	Sample Type	Rock type	SiO_2	TiO_2	Al_2O_3	Fe_2O_3	MnO	MgO	CaO	Na2O	K_2O	P_2O_5	LOI	Total
H23	Abida	10.05	40.73	Lava	Basalt	50.96	1.59	14.79	10.72	0.18	8.34	9.27	3.15	1.07	0.23	−0.47	100.30
H24	Abida	9.97	40.78	Lava	Basalt	51.61	1.27	22.40	7.52	0.12	2.10	11.21	3.50	0.92	0.21	−0.03	100.86
H25	Abida	9.94	40.87	Lava	Basalt	48.11	2.25	15.32	14.45	0.22	5.49	9.30	3.32	0.81	0.32	−0.18	99.60
H29	Abida	9.90	40.90	Lava	Basalt	48.37	2.34	15.12	12.51	0.19	8.07	12.01	2.45	0.42	0.30	−0.32	101.78
H32a	Abida	9.90	40.90	Lava	Basalt	48.63	2.17	15.79	13.69	0.21	6.23	9.83	3.26	0.78	0.29	−0.42	100.89
H32b	Abida	9.90	40.90	Lava	Basalt	48.74	2.29	15.75	14.14	0.22	5.30	9.07	3.43	0.91	0.33	−0.49	100.18
H35	Abida	9.90	40.90	Lava	Basalt	48.12	2.44	14.83	12.70	0.19	6.96	11.75	2.53	0.40	0.33	0.03	100.26
H36	Abida	9.90	40.89	Lava	Basalt	49.88	1.69	17.00	11.30	0.18	5.75	10.96	3.00	0.89	0.24	−0.43	100.90
H43	Abida	10.06	40.95	Lava	Basalt	48.88	2.38	14.68	13.47	0.21	6.34	9.28	3.29	0.92	0.31	−0.41	99.77
H46	Abida	10.07	40.87	Lava	Trachyandesite	56.61	1.77	14.74	10.88	0.22	2.01	5.39	4.78	2.51	0.52	−0.56	99.42
H47	Abida	10.07	40.86	Lava	Rhyolite	69.13	0.38	14.30	4.78	0.15	0.22	1.20	5.76	4.06	0.03	−0.18	100.03
H48	Abida	10.06	40.84	Lava	Basalt	50.61	2.46	15.56	12.87	0.21	3.89	9.14	3.71	1.11	0.40	−0.55	99.97
H50	Abida	10.06	40.82	Lava	Trachyte	66.30	0.50	14.76	5.20	0.20	0.41	1.71	6.31	3.90	0.05	−0.03	99.33
H52	Abida	10.07	40.85	Lava	Trachyte	64.31	0.80	15.03	7.44	0.20	0.72	2.79	5.61	3.33	0.17	−0.06	100.40
H53	Abida	10.13	40.89	Lava	Rhyolite	69.91	0.31	11.77	5.63	0.14	0.14	0.60	5.48	4.30	0.01	0.16	98.28
H54	Abida	10.13	40.84	Tuff	Trachytic Tuff	61.24	0.84	16.26	7.05	0.20	1.27	4.33	5.97	2.41	0.14	0.33	99.72
H12	Ayelu	10.07	40.62	Tuff	Rhyolite Tuff	70.49	0.19	13.31	3.29	0.10	0.11	2.25	4.97	4.90	0.01	3.97	99.65
H13	Ayelu	10.11	40.64	Tuff	Trachytic Tuff	67.71	0.31	13.24	4.79	0.17	0.11	1.25	5.53	4.09	0.03	0.22	99.23
H14	Ayelu	10.13	40.64	Tuff	Rhyolitic Tuff	69.35	0.21	14.56	3.45	0.11	0.14	0.86	4.76	5.01	0.04	3.51	98.50
H15	Ayelu	10.18	40.66	Lava	Basalt	48.42	1.70	16.40	11.40	0.18	7.61	11.19	2.78	0.69	0.23	−0.33	100.60
H17	Ayelu	10.17	40.68	Tuff	Rhyolitic Tuff	72.58	0.21	13.79	3.48	0.11	0.09	0.63	5.70	4.41	0.02	0.25	101.30
H18a	Ayelu	10.17	40.69	Tuff	Rhyolitic Tuff	71.37	0.25	13.76	3.61	0.10	0.31	1.12	5.46	4.33	0.03	0.34	101.35
H18b	Ayelu	10.17	40.69	Tuff	Rhyolitic Tuff	71.13	0.20	13.44	3.33	0.10	0.33	0.89	5.59	4.31	0.05	0.44	99.37
H57	Ayelu	10.09	40.69	Tuff	Rhyolitic Tuff	70.54	0.21	14.15	3.46	0.10	0.08	0.80	5.08	4.70	0.00	3.51	99.14
H59a	Ayelu	10.13	40.69	Tuff	Rhyolitic Tuff	71.47	0.31	13.04	4.63	0.14	0.05	0.71	5.62	4.40	0.02	0.20	100.38
H59b	Ayelu	10.13	40.69	Tuff	Rhyolitic Tuff	71.46	0.30	13.02	4.51	0.14	0.06	0.73	5.50	4.41	0.01	0.14	100.16
H9	Ayelu	9.98	40.55	Lava	Basalt	48.09	1.92	15.89	11.64	0.18	7.48	11.58	2.73	0.60	0.28	−0.59	100.38
H345	Yangudi	10.67	41.02	Tuff	Rhyolitic Tuff	69.45	0.24	15.39	3.75	0.13	0.06	0.90	5.96	3.85	0.01	0.31	99.73
H350	Yangudi	10.67	41.02	Lava	Basalt	49.81	3.77	13.89	15.48	0.27	4.28	8.54	3.68	0.89	0.47	−0.51	101.06
H352	Yangudi	10.67	41.04	Lava	Trachybasalt	50.99	3.10	13.76	14.72	0.27	3.38	7.86	3.93	1.15	0.54	−0.38	99.69
H354	Yangudi	10.67	41.04	Lava	Basalt	48.78	2.32	17.23	11.77	0.19	3.78	11.04	3.18	0.78	0.40	0.22	99.46
H355	Yangudi	10.67	41.05	Lava	Basalt	47.45	2.15	15.70	11.31	0.17	7.78	11.82	2.49	0.42	0.26	−0.24	99.55
H358	Yangudi	10.65	41.06	Lava	Basalt	47.83	2.29	15.44	13.05	0.19	6.38	11.03	2.90	0.55	0.26	−0.64	99.91
H360	Yangudi	10.61	41.04	Lava	Rhyolite	72.54	0.25	11.86	4.64	0.12	0.04	0.30	5.59	4.32	0.01	0.08	99.66
H363	Yangudi	10.60	41.06	Lava	Basalt	47.73	2.88	14.46	14.36	0.23	5.79	9.64	3.41	0.72	0.40	−0.28	99.60
H368	Yangudi	10.59	41.03	Lava	Basalt	50.16	2.35	16.42	12.57	0.22	3.64	9.21	3.66	1.04	0.51	−0.25	99.78
H374	Yangudi	10.58	41.04	Lava	Basalt	48.11	1.51	21.98	8.31	0.12	3.70	13.07	2.71	0.44	0.19	−0.21	100.15
H376	Yangudi	10.56	41.03	Lava	Rhyolite	70.49	0.33	13.48	5.12	0.16	0.05	1.14	5.80	3.81	0.01	0.28	100.40
H377	Yangudi	10.55	41.03	Lava	Trachyandesite	56.70	1.70	13.56	13.46	0.28	1.50	5.08	4.82	2.28	0.60	−0.30	99.97
H381	Yangudi	10.56	41.01	Lava	Basalt	46.50	1.81	18.88	9.56	0.14	4.30	12.68	2.68	0.50	0.22	0.30	97.24
H385	Yangudi	10.53	41.00	Lava	Basalt	48.65	2.49	14.70	13.48	0.23	6.57	9.33	3.33	0.80	0.55	−0.78	100.13
H387	Yangudi	10.54	40.97	Lava	Basalt	48.44	2.86	16.02	12.27	0.19	5.65	10.75	3.09	0.72	0.41	−0.53	100.40
H398	Yangudi	10.52	41.04	Lava	Basalt	49.87	2.97	14.40	13.53	0.22	4.93	8.68	3.65	0.99	0.62	−0.48	99.85
H399	Yangudi	10.52	41.04	Lava	Basalt	48.35	3.40	13.79	15.32	0.26	4.28	8.99	3.58	0.98	0.86	0.08	99.83
H402	Yangudi	10.61	41.10	Lava	Basaltic Trachyandesite	54.23	2.37	14.18	12.95	0.24	2.68	6.56	4.34	1.59	0.73	0.13	99.86

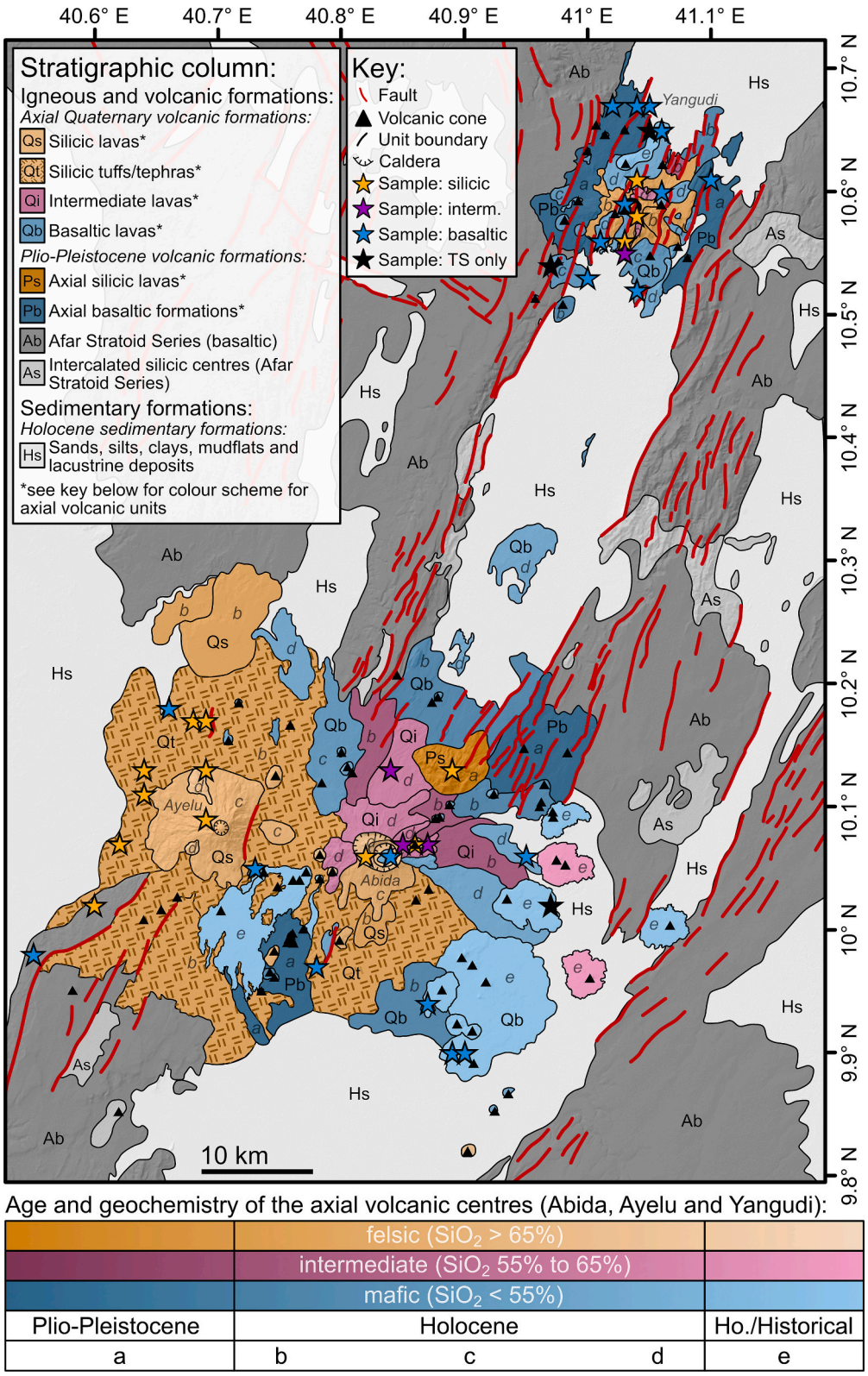

Fig. 4. Geological map of Abida, Ayelu and Yangudi based on remote sensing observations, with relative ages derived from cross-cutting relationships and absolute ages derived from previously published maps and stratigraphic descriptions from Varet (1975). Major geological and volcanic units are shown, along with major faults, cones, and sample localities. Approximate stratigraphic ages, unit names and unit descriptions are modified from Varet (1975). TS only = thin section only (i.e. no rock sample), interm. = sample of intermediate silica composition, Ho./Historical = Holocene/Historical. Sample compositions are based on XRF data. Sample names for the sample sites shown are provided in close-up maps shown in Figs. 5 and 6, and sample names and locations (in degrees latitude/longitude) are provided in both Table 1 and in the Supplementary Material (Supplementary Material 1).

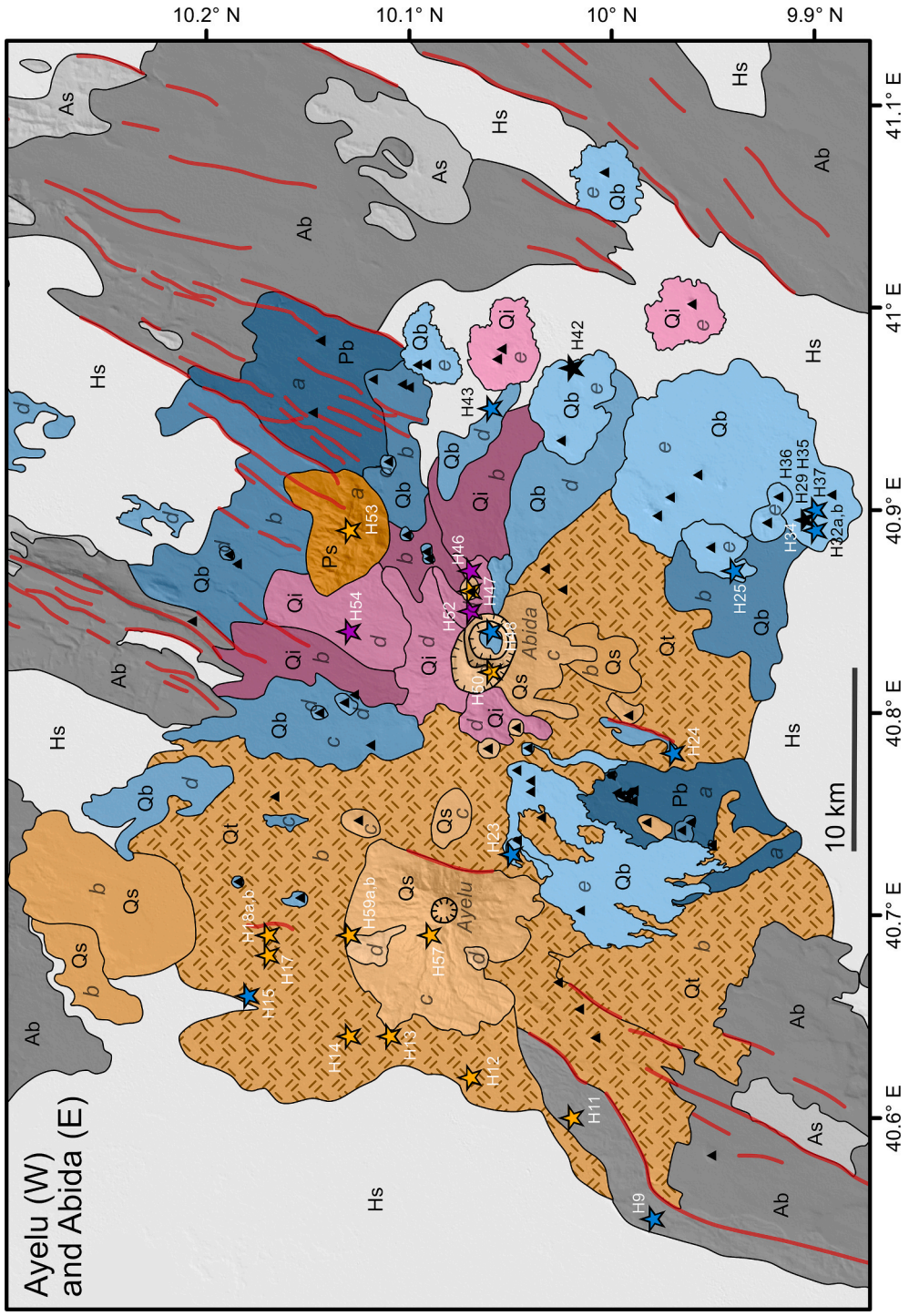

Fig. 5. Geological map close-up section of Ayelu (W) and Abida (E) (from Fig. 4), showing geological units, sample locations, and sample names. See Fig. 4 for detailed key and explanations.

and western flanks of Abida, as well as much of the immediate area surrounding Ayelu. These deposits are typically a paler red-and-yellow colour compared to the lava flows, and in places the surface show a moderate amount of re-working through surficial sedimentary processes. Small vegetation-lined ephemeral streams cut through this unit, transporting rainfall and loose material from Ayelu and Abida into the Awash Valley to the west.

With a maximum elevation of 2145 m, the prominent conical peak of Ayelu is formed of a succession of short (up to 4 km long) viscous felsic lava flows originating from the summit region. These flows form a steep-sided (c. 13°) cone with a diameter of around 10 km. These flows appear to postdate an older circular summit caldera (1.2 km diameter), the structure of which is now mostly obscured by overspilling lava flows and a post-caldera dome in the centre. The steep upper slopes of Ayelu are incised with deep valleys (up to 200 m deep), which form in a radial pattern around the summit. Several small landslip scarps (150 m wide) can be seen on the northern and north-western flanks of the volcano. Erosion, sediment cover and vegetation growth make it difficult to pick out any surface textures or indeed many individual lava flows – other than directly to the north, where measured estimates of the largest lobe

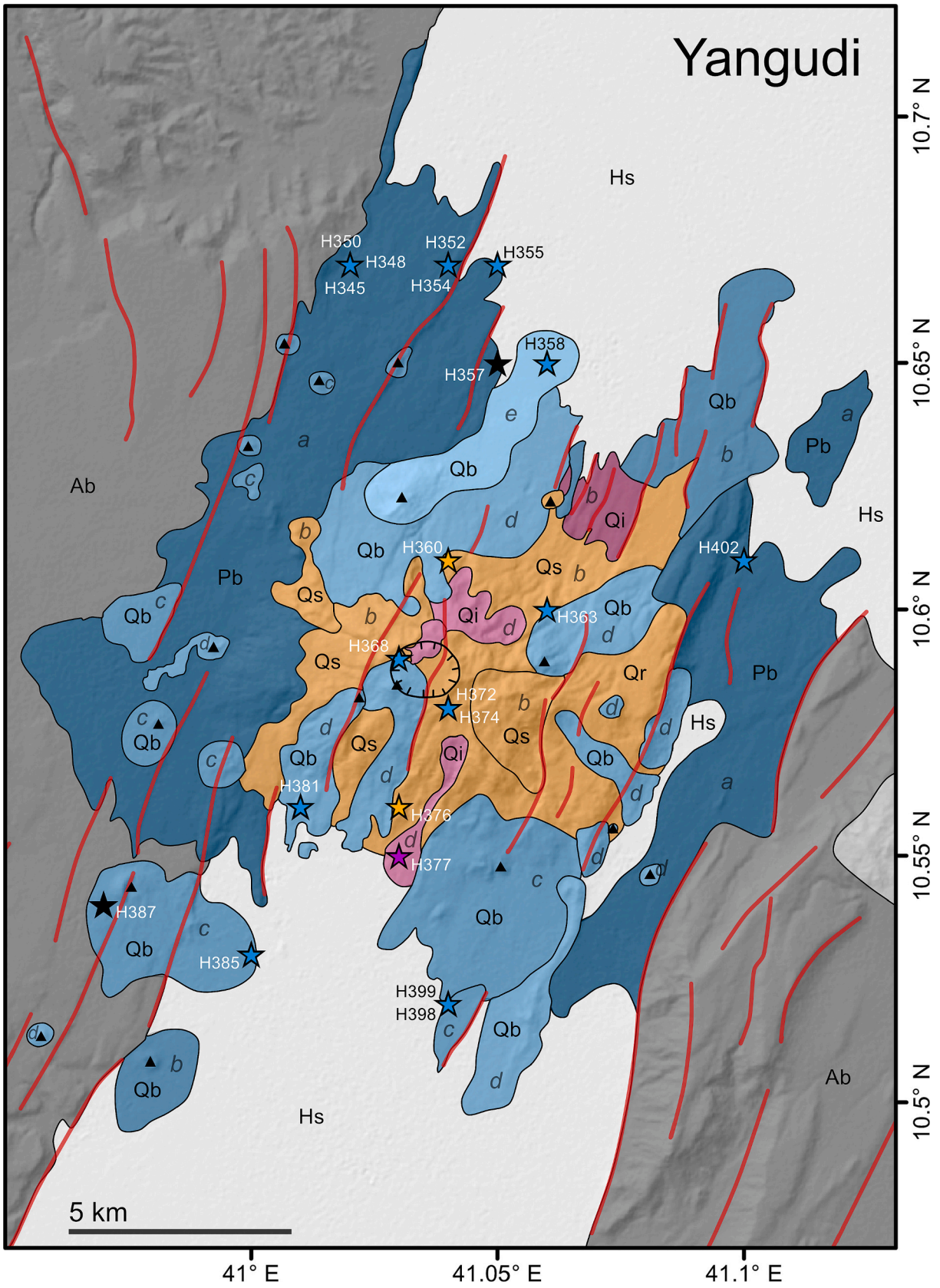

Fig. 6. Geological map close-up section of Yangudi (from Fig. 4), showing geological units, sample locations, and sample names. See Fig. 4 for detailed key and explanations.

give a maximum of 80 m flow thickness and a maximum volume estimate of >0.1 km^3.

Similarly, the summit region of Abida is formed of short (5–10 km long) lava flows, typically felsic to the south, and intermediate-basaltic to the north and east of the summit. Many of these intermediate and basaltic flows appear to have originated from the upper flanks of Abida, some 5 km from the summit. The intermediate and basaltic flows are typically blocky in texture, with some ropey pahoehoe-like textures visible in the centre of some of the larger flows. Like at Ayelu, sediment cover and erosion make it difficult to pick out many detailed features or flows. Unlike the conical peak of Ayelu, the summit of Abida is instead dominated by a large oval caldera (4 × 3 km, slightly elongated in the ESE-WNW direction), which contains a smaller circular caldera (diameter 2.5 km) within it – thought to have been formed as result of the large explosive tuff eruptions (Varet, 2017). A small basaltic dome grows within the centre of this smaller caldera. With a lower maximum elevation (1670 m) and a shallower slope angle (c. 8°), the morphology of Abida's slopes is less dominated by steep valleys and landslip scarps compared to its sibling Ayelu.

Stage 3: Late Holocene volcanism (post-caldera recent and historical). At Ayelu, volcanic activity ceased by the late Holocene – no evidence for recent volcanic activity is observed. Instead, recent, and late Holocene volcanic activity in the southern AMS is found only to the south and east of Abida. Of these recent deposits, only one is on the flanks of Abida proper, the other six are found between 10 km and 25 km to the east/southeast of the main summit. All seven of these recent deposits are basaltic or intermediate in compositiosn, are mid brown to dark brown-black in colour, and typically exhibit a blocky a'a surface texture. In two distinct localities (10.06°N, 40.98°E and 9.93°N, 40.89°E) the lavas form thick, ring-like ogive structures indicative of viscous lavas (Hunt et al., 2019).

Three of the seven recent deposits appear to be singular monogenetic scoria cones with an associated lava flow. These cones are typically between 60 m and 80 m tall, up to 650 m in diameter, and have very steep slope angles of up to 40°. The associated lava flows have a surface area of up to 20 km^2, but maximum thicknesses of no more than around 30 m, giving a maximum volume estimate of around 0.5 km^3. The other four recent deposits appear to be lava flows associated with two or more cones in close proximity to one another, such that it is difficult to say which of the cones the lava flows are associated with. These flows are spatially extensive, covering areas up to 35 km^2. However, with fairly flat elevation profiles typically not exceeding 60 m above the surrounding ground level, these flows are still small in volume with a maximum volume estimated to be on the order of around 0.7 km^3 for the largest compound flow.

As there is no physical overlap between the seven lava flows, it is not possible to suggest a relative age order based on cross-cutting relationships. However, overall, we can infer that with time there is a shift in volcanic activity to the far east of the southern AMS. Again, some of these recent lavas from Abida are believed to be only a few hundred years old (Global Volcanism Program, 2013). Specifically, the Global Volcanism Program lists 'uncertain' eruptions in 1828 and/or 1928, which would potentially align with a temporal clustering of fissural eruptions across multiple segments of the MER (Siegburg et al., 2023).

4.1.2. Volcanic evolution of Yangudi

Stage 1: Plio-Pleistocene rift floor basalts. Like Ayelu and Abida, Yangudi lies on a base of Plio-Pleistocene lavas, which can be seen in large outcrops both to the east and the west of the main volcanic centre. The earliest basaltic flows overlie the Udukya Plateau (the Afar Stratoid Series, Varet, 1975) on the western margin of the Adda'do Graben, suggesting that the formation of the volcano began before the formation of the axial graben. This unit is mid-red-brown in colour and appears to be heavily weathered. It is overlain in many places by significant amounts of recent sedimentary material, obscuring any evidence for individual flows within the unit. Networks of small ephemeral streams channel material westwards into the small sedimentary basins within the Udukya Plateau (Afar Stratoid Series) and northwards into the northern basin of the Adda'do Graben. Morphometrically, the lavas appear to form elongate NNW-SSE (parallel to rift axis/graben axis) ridges, suggesting the lavas were erupted as part of a rift opening sequence/sourced from opening rifts.

Stage 2: Holocene volcanism. Unlike Ayelu and Abida, which are dominated by substantial Holocene tuff deposits, Yangudi is mainly comprised of accumulations of thick lava flows. Early Holocene basaltic lavas can be seen to the north and south of the main summit. These lavas are dark brown-black and blocky and appear weathered, with a significant amount of sedimentary cover. Overlaying these lavas and forming most of the volume of present-day Yangudi, is a series of thick rhyolitic flows. Typically pale in colour, there flows are generally too weathered to discern many specific flow characteristics or source origins. They appear to form thick layered drapes which build up the bulk of the volcano and appear to originate from sources across the entire width of the Adda'do Graben, rather than just from the central main volcano summit.

In addition to the rhyolitic flows, there are some slightly younger basaltic and intermediate flows. These flows are mainly associated with small cones on the upper flanks/summit region of Yangudi. Typically no more than 5 km long, these flows are dark red-brown in colour, and morphometrically are typically 'flatter' (i.e. thinner) than their rhyolitic counterparts. The morphology of these flows is heavily influenced by the pre-existing topography upon which they were erupted – they flow around existing thick rhyolite lavas and flow down fault scarps. To the south of the main summit are several basaltic flows, not directly part of the main volcano, which appear to be associated with faulting at the graben margins. These too are small, <3 km across on the longest axis and are dark brown-black in colour.

Several faults, parallel to the trend of the rift axis, cut through Yangudi. These faults can show substantial vertical offset, with up to 70 m vertical throw in places. In some cases, this faulting pre-dates the lava flows, as the lavas are observed to flow down fault scarps. However, in other locations the faulting clearly cuts through and offsets the lava flows (e.g., 10.586°N, 41.023°E). This observation suggests that magmatism and extensional faulting occurred simultaneously at Yangudi. These through-cutting faults, in combination with the thick layered drapes of lava flows which form the majority of Yangudi, gives this volcano an overall very complex and irregular profile when compared to the smooth steep-sided conical shapes of Ayelu and Abida.

Stage 3: Late Holocene volcanism (post-caldera recent and historical). Compared to Ayelu and Abida, relatively little recent activity occured at Yangudi. The only recent eruptive activity comprises a cone and an associated lava flow, found 4 km north of the main summit of Yangudi. The cone lies on the lower flanks of the volcano, where it overlaps with the western margins of the Adda'do Graben. The cone is moderately elongated in the NE-SW direction and is 1.7 km long and around 250 m tall. It is pale and ashy in appearance, with a prominent landslip scarp on its NW flank. Emerging to the NE from the cone is a dark lava flow, 4.6 km long, which runs down the north-eastern side of Yangudi and spills out into the northern Adda'do Graben basin. The lava is dark in colour and basaltic in composition and is formed of several successive lobes that breached one another as the lava travelled downslope. Large quantities of sediment, presumed pyroclastic material sourced from the cone, are washed down the central channel of the lava flow. Bounded by the levees of the lava flow, this sedimentary material is efficiently transported northwards over the lava flow and into the basin to the north. This material obscures all but the most distal lobe of the lava flow, which forms a wide (1.3 km) but flat (10 m) fan shape.

4.2. Major element geochemistry and petrology

Classification of the whole-rock samples from Ayelu, Abida and Yangudi (after Le Bas et al., 1986) show a full suite of rock types from

basalts to rhyolites, including a range of intermediate compositions (Table 1, Fig. 7a). All three volcanoes exhibit both felsic and mafic endmembers (Abida: SiO_2 48 wt% to 70 wt%, Ayelu: SiO_2 48 wt% to 73 wt%, Yangudi: SiO_2 47 wt% to 73 wt%). Although the compositional distribution at Yangudi and Abida is broadly bimodal, these volcanoes also have a small number of intermediate compositions. The majority of the 45 rocks analysed in this study are basaltic lavas (24), with eight intermediate rocks (including two tuffs) and 13 felsic rocks (including nine tuffs). The samples follow a slightly tholeiitic trend, with most of the samples sitting on or just below the alkaline/tholeiitic line defined by Irvine and Baragar (1971). Total alkaline content and $Na_{8.0}$ values put the AMS samples in line with other volcanoes from Afar (Barrat et al., 1998; Ferguson et al., 2013; Field et al., 2013) (Fig. 7a, b).

Bivariate Harker diagrams (Fig. 8) show the variations of major elements for Ayelu, Abida and Yangudi, with respect to MgO. SiO_2, K_2O and Na_2O content tend to decrease with MgO, whereas CaO, Fe_2O_3, P_2O_5 and TiO_2 broadly increase with MgO, though with a wider range of values at the high MgO (basaltic) end of the spectrum. Al_2O_3 generally increases with MgO, but with several outliers. Ayelu is slightly less sodic and slightly more potassic than the other two volcanoes, and Yangudi shows a slight enrichment in P_2O_5, TiO_2 and MnO. However, the general trends for all three volcanoes are very similar to one another, suggesting similar patterns of melt evolution at each. Further, they lie within the range from other volcanoes from Afar and the MER (Fig. 7).

Representative photomicrographs for eight selected thin section samples are shown in Fig. 9. Modal mineral abundances for the 41 thin section are summarised in Table 2. The majority of the samples (28) are variably porphyritic basalts/microgabbros (phenocryst content 0–60% area; mean 22%), with the dominant phenocryst phases of plagioclase, followed by K-feldspar and pyroxene. Tuff samples typically contain few phenocrysts (3–5% area), with the dominant phenocryst phase being orthoclase.

5. Discussion and conclusions

5.1. Evolution of Ayelu, Abida and Yangudi volcanoes

Although considerably different in morphology and size, Abida, Ayelu, and Yangudi appear to have followed a broadly similar compositional evolution (Fig. 10). All three volcanoes are underlain by Plio-Pleistocene basaltic lavas erupted from rift fissures. All the volcanoes have developed to erupt larger volumes of a more evolved rhyolitic flows and/or ignimbrites (estimated to be in the order of magnitude of up to 10s of km^3 for ignimbrites erupted by Ayelu) (Figs. 4–7 and 10). Recent post-caldera activity at all three volcanoes is dominated by basaltic and intermediate lava flows, generally originating from satellite cones or fissures on or around the volcano flanks (Figs. 4–6 and 10). At each volcano, both felsic and mafic endmembers are found (Fig. 7), and at Yangudi and Abida we observe an almost complete magmatic sequence from basalts to rhyolites including intermediate compositions (Fig. 7). The compositions of some of these rocks are alkaline in composition (Fig. 7), in line with other Afar/MER Quaternary volcanoes (e.g. Ayalew et al., 2016; Hutchison et al., 2018; and references therein).

We now discuss the evolution of Abida, Ayelu, and Yangudi, and the relationships between them. We discuss Ayelu/Abida and Yangudi separately because of their spatial separation (Fig. 1), which hampers attempts to make comparisons on their relative ages, and their differing tectonic settings (lateral rift step versus the axial and latitudinal centre of the magmatic segment).

5.1.1. Ayelu and Abida

Deposits from the centres of Ayelu and Abida overlap (Fig. 5), and as a result have even been described as belonging to one system (e.g. Tesfaye et al., 2003; Ayele et al., 2006; Varet, 2017). Based on remote sensing observations, the presence of two nested calderas on Abida provide evidence for at least two series of mafic-to-felsic evolution at

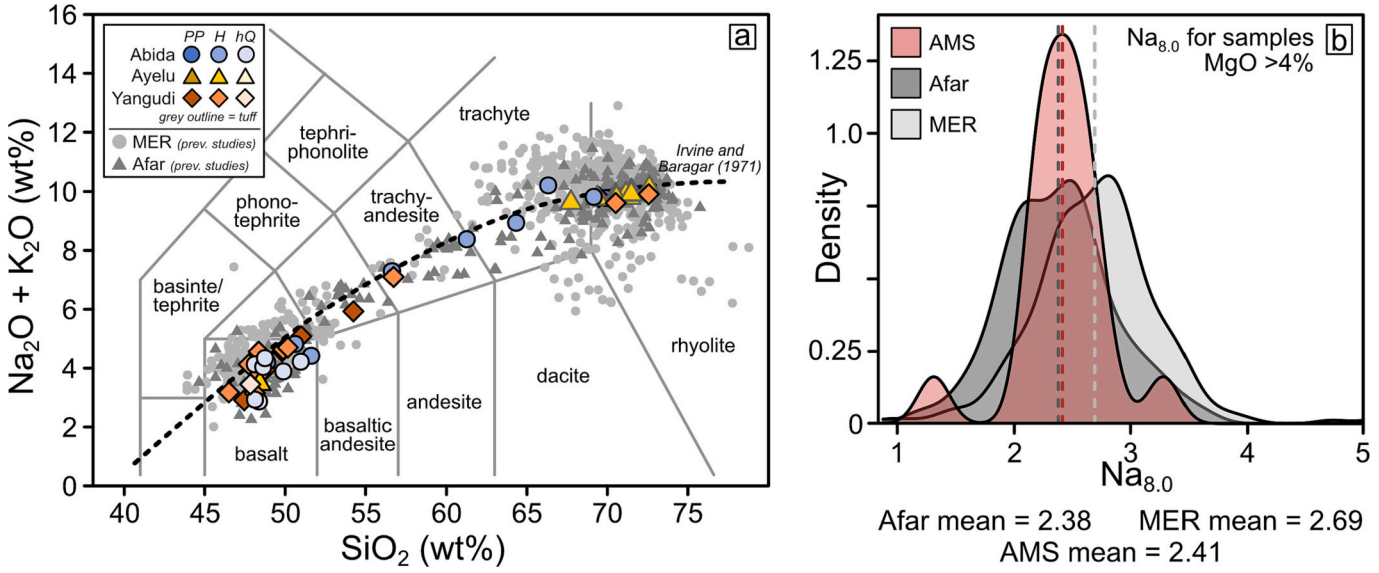

Fig. 7. (a) Total Alkali-Silica diagram (after Le Bas et al., 1986) showing the whole rock compositions of 44 samples from Abida, Ayelu and Yangudi (this study, coloured points). Symbol shapes and colours refer to the volcano from which the sample originates (Yangudi = red diamond, Abida = blue circle, Ayelu = yellow triangle), colour shading refers to sample age (darkest = Plio-Pleistocene/PP, mid shades = Holocene/H, lightest = late/historical Quaternary/hQ). Dashed line shows the division of volcanic rocks into alkaline (above) and subalkaline/tholeiitic (below), after Irvine and Baragar (1971). Selected published whole rock Quaternary volcanic rocks from MER (Hertali, Dofan, Fantale, Kone, BBVC, Gudda, Bishoftu, Gedemsa and Aluto; pale grey circles) and Afar (Badi, Erte Ale and Dabbahu; mid grey triangles) are shown. Published data are from Bizouard et al., 1980; Brotzu et al., 1980b; Brotzu et al., 1980a; Gasparon et al., 1993; Webster et al., 1993; Wolde and Widenfalk, 1994; Boccaletti et al., 1995; Barrat et al., 1998; Barberio et al., 1999; Peccerillo et al., 2003; Rooney et al., 2005, 2007; Furman et al., 2006; Ronga et al., 2010; Rooney et al., 2012a; Rooney et al., 2012b; Ferguson et al., 2013; Field et al., 2013; Giordano et al., 2014; Ayalew et al., 2016; Hutchison et al., 2016a, 2016b; and Siegburg, 2019. (b) density plot of $Na_{8.0}$ (where $Na_{8.0} = Na_2O + 0.373*MgO - 2.98$, after Klein and Langmuir, 1987) for Afar, MER and AMS volcanoes, for samples where MgO > 4%. (For interpretation of the references to colour in this figure legend, the reader is referred to the web version of this article.)

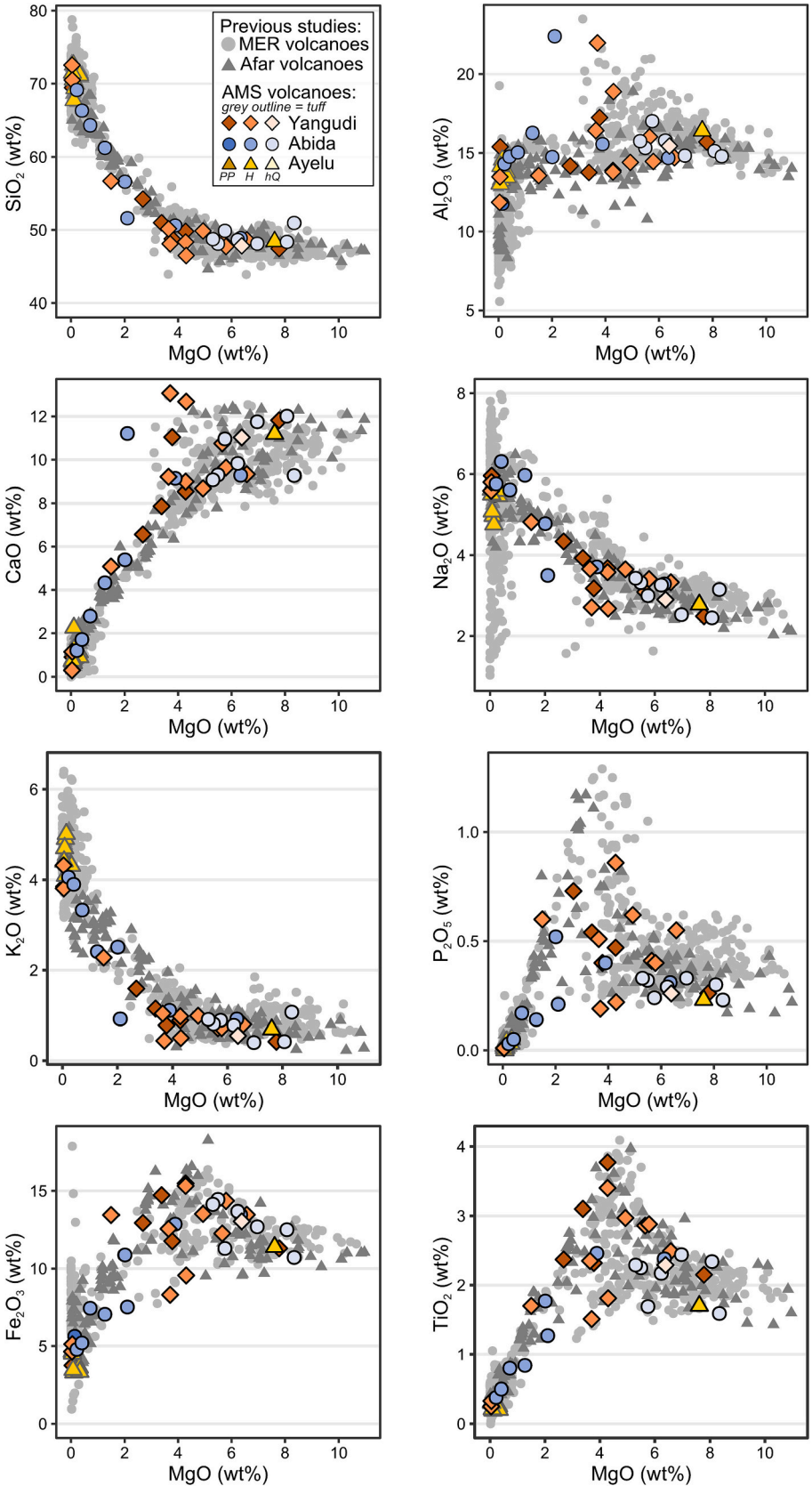

Fig. 8. Major element bivariant diagrams showing the whole rock compositions of 45 samples from Abida, Ayelu and Yangudi (this study, coloured points). Symbol shapes and colours refer to the volcano from which the sample originates (Yangudi = red diamond, Abida = blue circle, Ayelu = yellow triangle), colour shading refers to sample age (darkest = Plio-Pleistocene/PP, mid shades = Holocene/H, lightest = late/historical Quaternary/hQ). Selected published whole rock Quaternary volcanic rocks from MER (Hertali, Dofan, Fantale, Kone, BBVC, Gudda, Bishoftu, Gedemsa and Aluto; pale grey circles) and Afar (Badi, Erte Ale and Dabbahu; mid grey triangles) are shown. Published data are from Bizouard et al., 1980; Brotzu et al., 1980b; Brotzu et al., 1980a; Gasparon et al., 1993; Webster et al., 1993; Wolde and Widenfalk, 1994; Boccaletti et al., 1995; Barrat et al., 1998; Barberio et al., 1999; Peccerillo et al., 2003; Rooney et al., 2005, 2007; Furman et al., 2006; Ronga et al., 2010; Rooney et al., 2012a; Rooney et al., 2012b; Ferguson et al., 2013; Field et al., 2013; Giordano et al., 2014; Ayalew et al., 2016; Hutchison et al., 2016a, 2016b; and Siegburg, 2019. (For interpretation of the references to colour in this figure legend, the reader is referred to the web version of this article.)

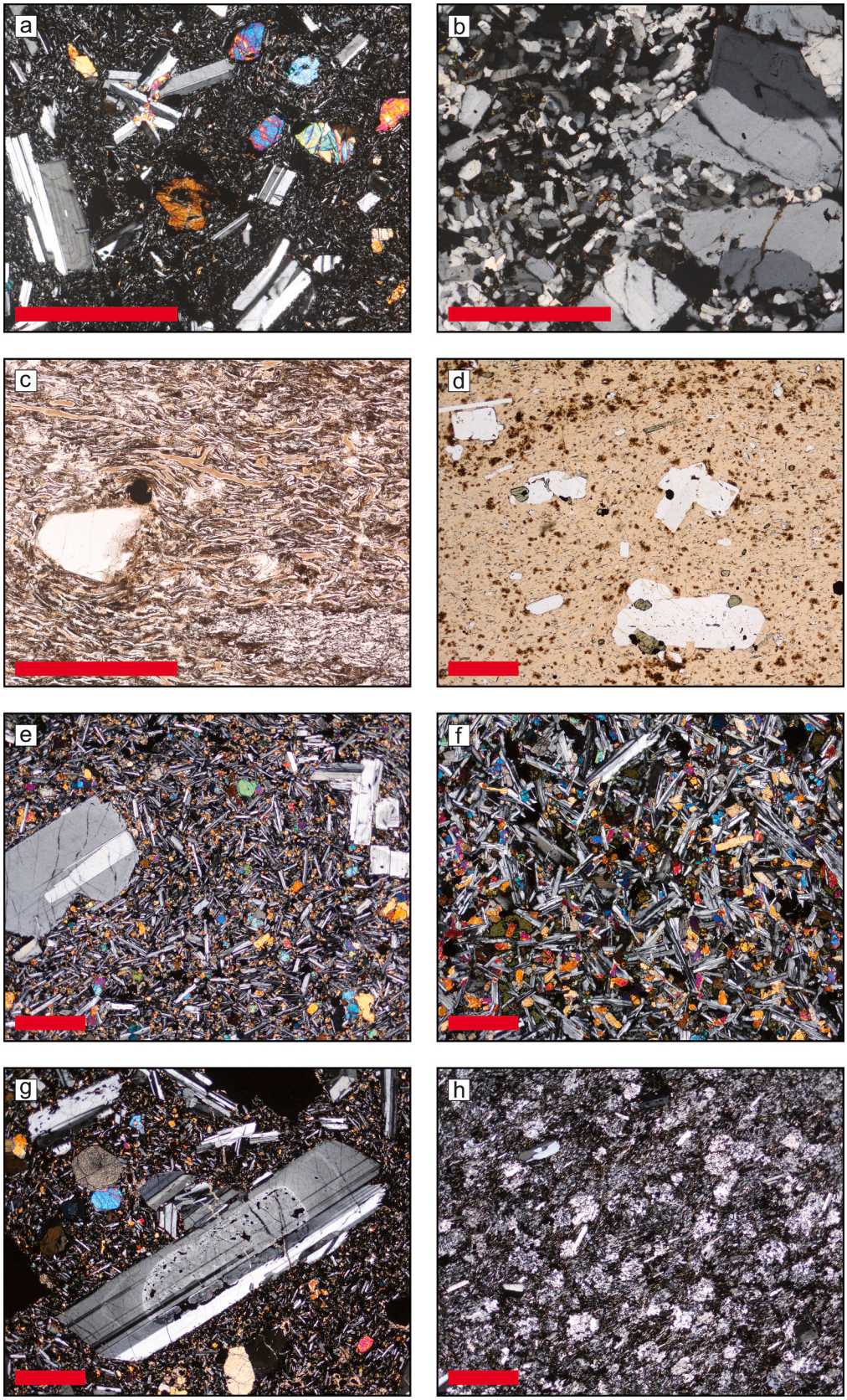

Fig. 9. Representative thin section photomicrographs from Abida, Ayelu and Yangudi, selected to showcase the variability in petrography from the Adda'do Graben volcanoes. (a) H25: very fine grained porphyritic basalt from a very recent (Quaternary/historical) lava flow from SE Abida. (b) H50: holocrystalline rhyolite from the caldera of Abida. (c) H11: welded tuff from a distal ignimbrite flow, SW Ayelu. (d) H13: glassy tuff from a distal ignimbrite flow, W Ayelu. (e) H15: porphyritic microgabbro from NW Ayelu. (f) H348: holocrystalline microgabbro from a recent (Quaternary) distal flow, NW Yangudi. (g) H354: porphyritic basalt from NW Yangudi, highlighting a range of disequilibria textures (thick oscillatory zoning, pitted core, and rim dissolution). (h) H360: holocrystalline rhyolite from the northern flank of Yangudi. Red scale bar in all photos is 1 mm. (For interpretation of the references to colour in this figure legend, the reader is referred to the web version of this article.)

Table 2
Modal abundances of major phenocryst phases for 41 thin sections analysed. Abundances are given in percentage surface area estimates (%SA). G'mass = groundmass, Plag = plagioclase, K-Feld = K-Feldspar, Ol = olivine, Cpx = clinopyroxene, Opx = orthopyroxene, Ox = opaque oxides, Amph = amphibole.

					Estimated modal abundances (percent surface area, %SA)										
Sample	Volcano	Latitude (°N)	Longitude (°E)	Brief description	Vesicles	G'mass	Xenoliths	Phenocrysts (T)	Plag	K-Feld	Ol	Cpx	Opx	Ox	Amph
H23	Abida	10.05	40.73	basalt, porphyritic	30	60	–	10	2	1	–	3	4	–	–
H24	Abida	9.97	40.78	basalt, porphyritic	2	68	–	30	19	5	–	2	3	1	–
H25	Abida	9.94	40.87	basalt, porphyritic	5	80	–	15	7	3	–	2	3	<1	–
H29	Abida	9.90	40.90	basalt, glassy g'mass	40	40	–	20	12	6	–	1	1	–	–
H32a/b	Abida	9.90	40.90	basalt, porphyritic	2	58	–	40	10	25	–	1	2	2	–
H36	Abida	9.90	40.89	microgabbro, porphyritic	10	30	–	60	30	10	<1	14	5	1	–
H43	Abida	10.06	40.95	basalt, porphyritic	14	80	–	6	3	2	–	1	<1	<1	–
H46	Abida	10.07	40.87	basalt, porphyritic	<1	85	–	15	7	3	–	3	1	1	–
H47	Abida	10.07	40.86	rhyolite, holocrystalline	–	90	–	10	–	8	–	<1	–	<1	1
H48	Abida	10.06	40.84	basalt, porphyritic	5	55	–	40	18	12	–	7	3	–	–
H50	Abida	10.06	40.82	rhyolite, holocrystalline	–	95	–	5	–	4	–	<1	–	–	1
H52	Abida	10.07	40.85	intermediate, porphyritic	–	88	–	12	2	6	–	1	1	<1	–
H53	Abida	10.13	40.89	rhyolite, holocrystalline	–	95	–	5	–	4	–	<1	–	–	1
H54	Abida	10.13	40.84	tuff, some crystals and xenoliths	5	82	5	8	2	4	–	2	–	–	<1
H12	Ayelu	10.07	40.62	welded tuff, very few phenocrysts	–	99	–	1	–	1	–	<1	–	–	<1
H13	Ayelu	10.11	40.64	glassy tuff, very few phenocrysts	–	95	–	5	–	4	–	1	<1	–	<1
H14	Ayelu	10.13	40.64	welded tuff, very few phenocrysts, xenoliths	–	97	2	1	–	1	–	<1	–	–	–
H15	Ayelu	10.18	40.66	microgabbro, holocrystalline	1	98	–	1	–	1	–	–	–	–	–
H17	Ayelu	10.17	40.68	welded tuff, very few phenocrysts, xenoliths	<1	98	2	<1	–	<1	–	–	–	–	–
H18a	Ayelu	10.17	40.69	welded tuff, very few phenocrysts, xenoliths	<1	96	3	1	–	1	–	<1	–	–	–
H18b	Ayelu	10.17	40.69	welded tuff, very few phenocrysts, xenoliths	–	98	1	1	–	1	–	–	–	<1	–
H57	Ayelu	10.09	40.69	welded tuff, very few phenocrysts, xenoliths	–	96	2	2	–	2	–	<1	–	–	–
H59a/b	Ayelu	10.13	40.69	welded/crystalline tuff, very few phenocrysts	3	94	–	3	–	2	–	<1	–	–	<1
H9	Ayelu	9.98	40.55	basalt, porphyritic	5	80	–	15	8	4	<1	1	2	<1	–
H345	Yangudi	10.67	41.02	holocrystalline basalt, occasional phenocryst	1	97	–	2	2	<1	–	–	–	–	–
H350	Yangudi	10.67	41.02	holocrystalline basalt, few microphenocrysts	2	98	–	<1	<1	<1	–	<1	<1	–	–
H352	Yangudi	10.67	41.04	holocrystalline basalt, few microphenocrysts	2	98	–	<1	<1	<1	–	<1	<1	–	–
H354	Yangudi	10.67	41.04	basalt, porphyritic	15	45	–	40	20	–	–	15	5	–	–
H355	Yangudi	10.67	41.05	basalt, porphyritic	5	60	–	35	20	–	–	10	5	–	–
H358	Yangudi	10.65	41.06	basalt, holocrystalline	5	92	–	3	1	2	–	–	–	–	–
H363	Yangudi	10.60	41.06	basalt, porphyritic	2	93	–	5	3	<1	–	2	<1	–	–
H368	Yangudi	10.59	41.03	basalt, porphyritic	15	45	–	40	20	5	2	8	5	–	–
H374	Yangudi	10.58	41.04	basalt, porphyritic	30	50	–	20	15	–		3	2	–	–
H376	Yangudi	10.56	41.03	holocrystalline basalt, occasional phenocryst	1	97	–	2	1	1	–	–	–	–	–
H377	Yangudi	10.55	41.03	holocrystalline basalt, occasional phenocryst	1	98	–	1	<1	<1	–	<1	<1	–	–
H381	Yangudi	10.56	41.01	basalt, porphyritic	20	40	–	40	28	5	–	4	3	–	–
H385	Yangudi	10.53	41.00	basalt, porphyritic	5	85	–	10	7	–	–	1	2	–	–
H387	Yangudi	10.54	40.97	basalt, porphyritic	10	75	–	15	10	–	–	3	2	<1	–
H398	Yangudi	10.52	41.04	holocrystalline basalt, few microphenocrysts	2	88	–	10	3	2	–	3	2	<1	–
H399	Yangudi	10.52	41.04	holocrystalline basalt	2	98	–	–	<1	–	–	<1	–	–	–
H402	Yangudi	10.61	41.10	holocrystalline basalt	5	95	–	–	<1	–	–	–	–	–	–

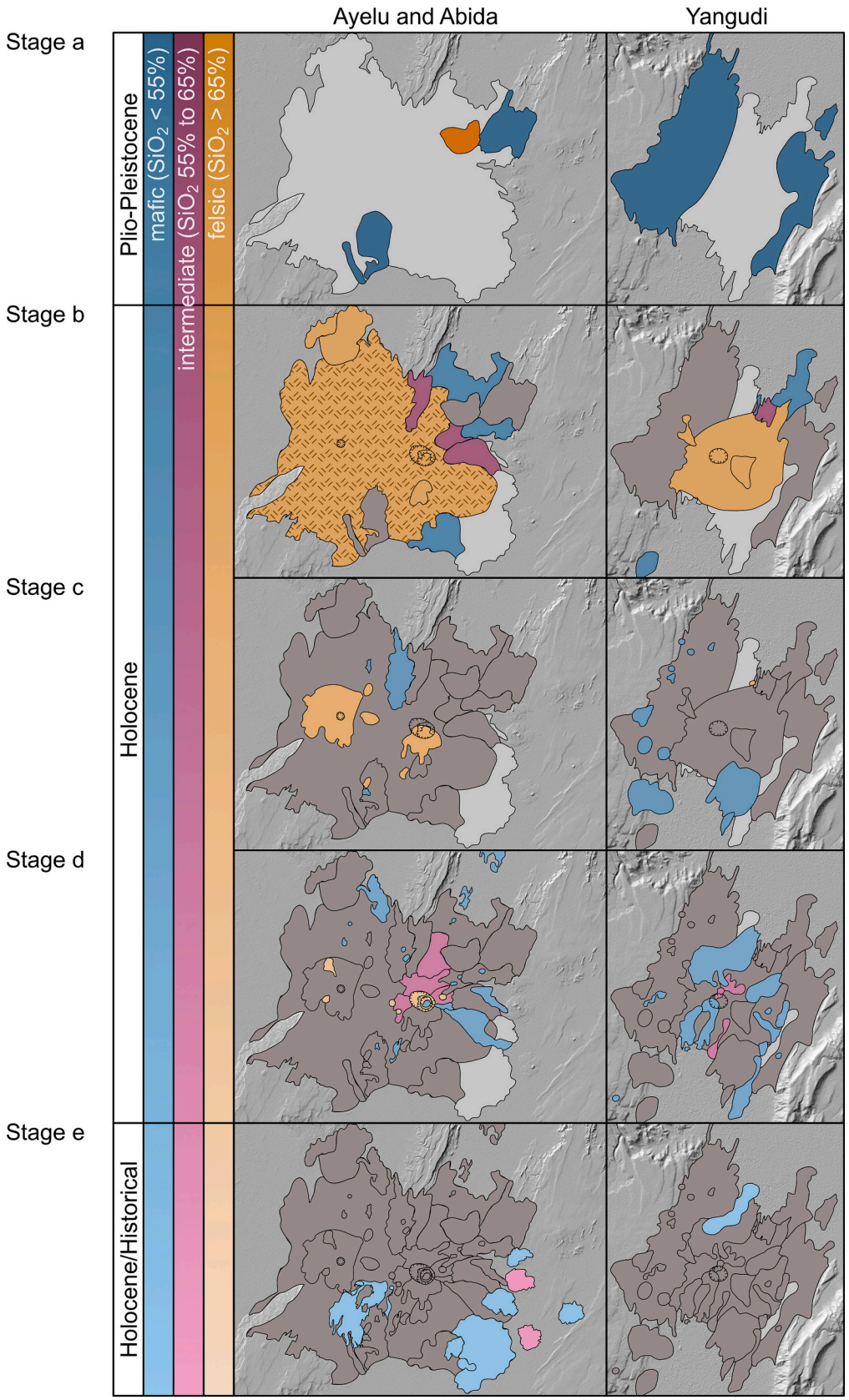

Fig. 10. Chronology of the evolutionary stages (a-e) of Ayelu, Abida (left) and Yangudi (right), based predominantly on cross-cutting relationships (see Section 3.1. Remote sensing mapping and geochronology for further details). Colours show rock composition based on SiO_2 content, solid fill indicates lava and patterned fill indicates tuff. Background imagery is hillshaded NASA SRTM DEM data.

Abida (pre- and post-caldera), which in turn overlie (i.e. post-date) rhyolitic sequences at Ayelu (Fig. 5). This provides evidence for at least three series of mafic-to-felsic evolution at Ayelu and Abida, suggesting the area has been a site of long-lasting volcanic activity, in agreement with an earlier study in this region (Varet, 2017). Based on observations from 3D flow relationships in Google Earth, ArcMap, and after Varet (2017), Ayelu is interpreted as being overall younger than Abida (Figs. 4–6). However, the most recent Quaternary/historical flows at these two volcanoes are exclusively from Abida, particularly on the eastern flank (Fig. 5). There appears to be a lateral eastward shift in volcanic activity at Ayelu and Abida, possibly related to movement and development along the across-rift fault zone upon which the two volcanoes lie (Fig. 2).

5.1.2. Yangudi

At Yangudi, a complete magmatic sequence from basalts to rhyolites, with intermediate compositions, is seen (Figs. 6 and 7). Notably, in contrast to Ayelu and Abida, the Yangudi system occurs in the centre of a graben (i.e., the Adda'do Graben; see Fig. 1). The earliest basaltic lavas (believed to be Pleistocene in age; Varet, 2017) overlie the plateau to the west, suggesting that the assembly of this volcano may have been initiated before the formation of the graben. To the east, however, these basaltic lavas instead abut the eastern wall of the graben. This could indicate an asymmetric development of the Adda'do Graben, or asynchronous fissure eruptions on the east and west sides of the graben during the late Pliocene. Despite the differences in tectonic setting of Yangudi relative to Ayelu-Abida, we do not observe any appreciable differences in the major element geochemistry of the deposits, which may imply similarities in the sub-volcanic magma assembly processes.

5.2. Evolution of the Adda'do Magmatic Segment (AMS)

Evidence for repeated mafic-to-felsic evoluntionary cycles within the AMS suggest it has long been an area of volcanic activity. Varet (2017) suggests an age of 500 ka (mid-Pleistocene) for lavas sampled at the base of the edifice of Ayelu, and though there are no absolute ages for Abida, Ayelu is generally considered to be the older of the two volcanoes (Mohr and Wood, 1976; Varet, 2017; Rooney, 2020a), suggesting at the oldest a mid-late Pleistocene age for Abida. There is no overlap of deposits from Ayelu/Abida and Yangudi (due to the 50 km distance between them), so it is not possible to use this to devise a relative stratigraphy between the northern and southern areas of volcanic activity in the AMS.

The vast majority of recent (late Holocene/historic) volcanic activity in the AMS appears to be concentrated in the southern AMS, in the form of several basaltic eruptions occurring 10–25 km away from the main centre of Abida. Similarly, recent volcanic activity at Yangudi occurs distally to the main centre, at a distance of around 8 km. Low-volume recent activity in the AMS is most likely associated with fissures along the graben border faults (Varet, 2017) – large build-ups of silicic melt storage underneath a volcanic centre have been known to deflect rising denser basaltic melt to a 'shadow zone' around the volcano (Mahood, 1984; Hutchison et al., 2016a; Fontijn et al., 2018), potentially resulting in more distal low-volume eruptions. Similar shadow zones are reported in other tectonic environments such as oceanic arcs and intraplate hotspots (Busby et al., 2023), for example the Cretaceuos Alistos Arc, Baja California (Busby et al., 2006), and Las Cañadas Caldera, Tenerife (Martí and Gudmundsson, 2000).

Most units at Yangudi are cut by axial-parallel faults (Fig. 6). Faults can be observed cutting units from Plio-Pleistocene to Holocene, suggesting that even some of the most recent volcanic activity at Yangudi pre-dates at least some of the faulting in this area. In contrast, this does not appear to be the case at Abida and Ayelu, where there is relatively little evidence for axial faulting cutting the erupted units (Fig. 5). Here, the lack of faulting could mean that Abida and Ayelu are on average younger than Yangudi, or that negligible axial faulting occurred at the lateral step in the rift where Ayelu and Abida lie (Fig. 2).

5.3. Evolutionary and geochemical comparison of Quaternary AMS volcanism to Quaternary MER and Afar volcanism

The Quaternary axial volcanic centres in the Northern MER and Southern Afar are predominantly silicic in composition (Fig. 7), and in most cases are characterised by large caldera-forming eruptions ($>>1$ km^3) at some point during their history (Hutchison et al., 2016a, 2016b; Rooney, 2020a, 2020b). Both the timings of these caldera-forming eruptions and the timings of post-caldera volcanism onset are poorly constrained for most volcanoes in this region, with the exception of new high-quality $^{40}Ar/^{39}Ar$ dates from Aluto, Kone, Fantale and Gedemsa (Hutchison et al., 2016b; Vidal et al., 2022) and the Boset-Bericha Volcanic Complex (BBVC) (Fontijn et al., 2018; Siegburg et al., 2018). Without any dates from Ayelu, Abida or Yangudi, it is challenging to make any direct temporal comparisons between the AMS volcanoes and others in the NMER and Afar. Instead, we focus our comparisons on the general evolutionary pathways and major element geochemistry trends between Quaternary volcanoes in the AMS, NMER, and Afar.

Detailed age studies from Aluto (Hutchison et al., 2016a, 2016b) suggest an early phase of edifice building at 150–400 ka, followed by major ignimbrite eruptions at c. 310 ka, and then episodic post-caldera volcanism at c. 60 ka, which followed a long period of quiescence lasting c. 250 ka. Similarly, at the BBVC, Siegburg et al. (2018) report early rift floor eruptions at c. >300 ka, followed by the formation of the volcanoes Gudda (including caldera formation; c. 120 ka) and Bericha (c. 14 ka), and more recent post-caldera activity (since c. 16 ka and c. 5 ka respectively). Between 320 and 140 ka, there are several significant major eruptive events in the NMER (Siegburg et al., 2018), including (but not limited to, see Siegburg et al., 2018 for a comprehensive summary) the aforementioned caldera collapse at Aluto at c. 310 ka (Hutchison et al., 2016b), magmatism and caldera collapse at Gedemsa (Bigazzi et al., 1993; Peccerillo et al., 2003), major ignimbrite eruptions at O'a (Mohr et al., 1980), Corbetti (Hutchison et al., 2016b) and Fantale (Williams et al., 2004). Best estimates suggest an approximate age of around 500 ka for lavas at the base of Ayelu (Varet, 2017), so it is entirely possible that the large caldera-forming eruptions from the younger Abida volcano fall within this 320–140 ka window. These broadly coeval large volcanic events across different magmatic segments in the MER could suggest a periodic supply of larger melt volumes in the region (Siegburg et al., 2018), possibly relating to a pulsing or heterogeneous mantle plume source (Parnell-Turner et al., 2014).

Although Ayelu and Abida are often regarded as two separate volcanoes in the literature, we can draw interesting parallels between them and other volcanic complexes in the MER with two closely located summits. For example, the BBVC comprises two main edifices, Gudda and Bericha, and appears to follow a broadly similar evolutionary pathway from early rift floor basalts, to evolved caldera-forming events, followed by post-caldera activity (Siegburg et al., 2018). At Ayelu and Abida, as in the BBVC with Gudda and Bericha, we see a 'switching' of volcanic activity between the edifices throughout time. This is expecially stark at Ayelu/Abida, where almost all post-caldera activity is associated with Abida (Fig. 10).

As the northernmost expression of the WFB, the AMS volcanoes appear spatially to be a direct northwards continuation of the NMER (Fig. 2). However, we observe that the major element trends of the AMS volcanoes generally more closely match those of other volcanoes in Afar than the MER (Figs. 7 and 8). Though there is considerable overlap between the major element trends from MER and Afar, compositions in Afar typically occupy a tighter sub-alkaline trend, whereas MER compositions tend to show more spread with a slightly higher tendency towards alkaline compositions (Fig. 7b). Crustal thickness beneath the AMS is similar to most of Afar (~25 km) (Maguire et al., 2006; Hammond et al., 2011), whereas crustal thickness along the MER increases significantly and abruptly just to the south of the AMS (Maguire et al., 2006) (Fig. 1). Similarly, lithospheric thickness increases by up to 40 km from Afar (50–70 km) to the MER (90 km) (Wong et al., 2022), resulting

in both a lower degree of partial melting and an increased depth of melting where the lithosphere is thicker (Niu, 2021). Melts produced at depth tend to be more alkalic (e.g. Stewart and Rogers, 1996) due to lower degree of partial melting (Putirka and Busby, 2007); therefore lithospheric thinning from the AMS northwards could explain lower alkalinities observed in the AMS and Afar volcanoes. However, further work such as isotopic analyses on samples from the AMS is required to fully test whether geochemical similarities between the AMS and Afar can be explained by lithospheric and crustal thickness variations alone, or whether plume-related mantle source heterogeneities play a role here too.

5.4. Conclusions

Here, we present for the first time major element geochemical analyses from 45 new whole-rock samples from the AMS volcanoes (Ayelu, Abida and Yangudi). We also used remote sensing techniques in ArcMap with a variety of datasets (satellite imagery and digital elevation models) to produce an updated geological map for the area, which enabled us to produce the first detailed relative geochronology for the AMS. Our key findings are summarised as follows:

- All three AMS volcanoes exhibit bimodal volcanism — observed in remote sensing analysis and confirmed by major element XRF analysis of whole-rock samples — and two of the three AMS volcanoes (Abida and Yangudi) also exhibit a range of intermediate compositions
- All three AMS volcanoes follow a similar evolutionary pattern, beginning with a base of Plio-Pleistocene lavas, followed by a volcano-building period of large volume evolved magmatism, and then recent/historical basaltic activity
- We find evidence for at least three cycles of mafic-to-felsic evolution at Ayelu-Abida, in agreement with earlier studies in the area (Varet, 2017), and we find that the timings of the large caldera-forming eruptions Abida likely fit within the same general 320–140 ka timescale as observed at other MER volcanoes (e.g. Aluto, BBVC, Corbetti, Gedemsa, Fantale and O'a; see Bigazzi et al., 1993; Peccerillo et al., 2003; Williams et al., 2004; Hutchison et al., 2016b; Siegburg et al., 2018)

Although this study represents a step forward in our understanding of volcanic processes in the NMER – Southern Afar, there remains much work to be done in the area. For example, other volcanoes in the region such as Gabillema (60 km north of the AMS) remain critically understudied. Furthermore, our current understanding of mantle sources and crust-mantle-plume interactions in this region is poor, and more work is required to better understand these processes in this volcanically active area.

CRediT authorship contribution statement

Rhiannon Rees: Writing – original draft, Methodology, Visualization, Investigation. **Thomas M. Gernon:** Conceptualization, Supervision, Writing – review & editing. **Derek Keir:** Conceptualization, Supervision, Resources, Writing – review & editing. **Rex N. Taylor:** Conceptualization, Supervision, Writing – review & editing. **Carolina Pagli:** Resources, Writing – review & editing.

Declaration of Competing Interest

The authors declare that they have no known competing financial interests or personal relationships that could have appeared to influence the work reported in this paper.

Data availability

All data supporting this study are openly available in the Supplementary Materials.

Acknowledgements

This work was funded by the Natural Environmental Research Council [grant number NE/S007210/1] as part of the INSPIRE Doctoral Training Program. DK acknoweldges Natural Environment Research Council (NERC) grant NE/L013932/1. DK and CP acknoweldge the Ministero dell'Università e della Ricerca (MiUR) through PRIN grant 2017P9AT72. TG was supported by The Alan Turing Institute under the EPSRC grant EP/N510129/1. We acknowledge the use of rocks from the Afar Repository of the University of Pisa (https://repositories.dst.unipi.it/index.php/home-afar), and would like to acknowledge the efforts and contributions of everyone involved in these 1970s sample collection expeditions in Afar.

We would like to thank the reviewers David Pyle and Cathy Busby for their detailed, helpful and constructive comments, which helped us improve the quality of this manuscript.

Appendix A. Supplementary data

Supplementary data to this article can be found online at https://doi.org/10.1016/j.jvolgeores.2023.107846.

References

Ayalew, D., Ebinger, C., Bourdon, E., Wolfenden, E., Yirgu, G., Grassineau, N., 2006. Temporal compositional variation of syn-rift rhyolites along the western margin of the southern Red Sea and northern Main Ethiopian Rift. Geological Society, London, Special Publications 259 (1), 121–130.

Ayalew, D., Jung, S., Romer, R.L., Kersten, F., Pfänder, J.A., Garbe-Schönberg, D., 2016. Petrogenesis and origin of modern Ethiopian rift basalts: Constraints from isotope and trace element geochemistry. Lithos 258, 1–14.

Ayele, A., Nyblade, A.A., Langston, C.A., Cara, M., Leveque, J.J., 2006. New evidence for Afro-Arabian plate separation in southern Afar. Geological Society, London, Special Publications 259 (1), 133–141.

Barberio, M.R., Donati, C., Donato, P., Yirgu, G., Peccerillo, A., Wu, T.W., 1999. Petrology and geochemistry of Quaternary magmatism in the northern sector of the Ethiopian Rift between Debre Zeit and Awash Park. Acta Vulcanologica 11, 69–82.

Barrat, J.A., Fourcade, S., Jahn, B.M., Cheminee, J.L., Capdevila, R., 1998. Isotope (Sr, Nd, Pb, O) and trace-element geochemistry of volcanics from the Erta'Ale range (Ethiopia). Journal of Volcanology and Geothermal Research 80 (1–2), 85–100.

Beyene, A., Abdelsalam, M.G., 2005. Tectonics of the Afar Depression: A review and synthesis. Journal of African Earth Sciences 41 (1–2), 41–59.

Bigazzi, B., Bonadonna, F.P., Di Paola, Giuliani, A., 1993. In: K-Ar and fission track ages of the last volcano tectonic phase in the Ethiopian Rift Valley (Tullu Moye area). In: Geology and mineral resources of Somalia and surrounding regions, 113. Istituto Agronomico Oltremare, Firenze, pp. 311–322.

Bizouard, H., Barberi, F., Varet, J., 1980. Mineralogy and petrology of Erta Ale and Boina volcanic series, Afar rift, Ethiopia. Journal of Petrology 21 (2), 401–436.

Boccaletti, M., Getaneh, A., Mazzuoli, R., Tortorici, L., Trua, T., 1995. Chemical variations in a bimodal magma system: the Plio-Quaternary volcanism in the Dera Nazret area (Main Ethiopian Rift, Ethiopia). Africa Geoscience Review 2 (1), 37–60.

Brotzu, P., Ganzerli-Valentini, M.T., Lincei, L., 1980a. Quaternary basaltic volcanism in the northern part of the main Ethiopian rift (from 8 to 9 Lat. N). Atti. Convegni. Lincei 47, 293–315.

Brotzu, P., et al., 1980b. Volcanological and magmatological evidence of the Boseti Volcanic complex (Main Ethiopian Rift). Atti. Convegni. Lincei 47, 317–366.

Busby, C., Adams, B.F., Mattinson, J., Deoreo, S., 2006. View of an intact oceanic arc, from surficial to mesozonal levels: Cretaceous Alisitos arc, Baja California. Journal of volcanology and geothermal research 149 (1–2), 1–46.

Busby, C.J., Morris, R.A., DeBari, S.M., Medynski, S., Putirka, K., Andrews, G.D., Schmitt, A.K., Brown, S.R., 2023. Geology of a Large Intact Extensional Oceanic Arc Crustal Section with Superior Exposures: Cretaceous Alisitos Arc, Baja California (Mexico). Geological Society of America Special Paper,, 560.

Casey, M.C.D.R.F.G., Ebinger, C., Keir, D., Gloaguen, R., Mohamed, F., 2006. Strain accommodation in transitional rifts: Extension by magma intrusion and faulting in Ethiopian rift magmatic segments. Geological Society, London, Special Publications 259 (1), 143–163.

Chernet, T., Hart, W.K., 1999. Petrology and geochemistry of volcanism in the northern Main Ethiopian Rift-southern Afar transition region. Acta Vulcanologica 11, 21–42.

Chernet, T., Hart, W.K., Aronson, J.L., Walter, R.C., 1998. New age constraints on the timing of volcanism and tectonism in the northern Main Ethiopian Rift–southern

Afar transition zone (Ethiopia). Journal of Volcanology and Geothermal Research 80 (3–4), 267–280.
Chorowicz, J., 2005. The east African rift system. Journal of African Earth Sciences 43 (1–3), 379–410.
Corti, G., 2009. Continental rift evolution: from rift initiation to incipient break-up in the Main Ethiopian Rift, East Africa. Earth-science reviews 96 (1–2), 1–53.
Corti, G., Bastow, I.D., Keir, D., Pagli, C., Baker, E., 2015. Rift-related morphology of the Afar Depression. Landscapes and Landforms of Ethiopia, pp. 251–274.
Ebinger, C., 2005. Continental break-up: the East African perspective. Astronomy & Geophysics 46 (2), 2–16.
Ebinger, C.J., Hayward, N.J., 1996. Soft plates and hot spots: Views from Afar. Journal of Geophysical Research: Solid Earth 101 (B10), 21859–21876.
Ebinger, C.J., Yemane, T., Woldegabriel, G., Aronson, J.L., Walter, R.C., 1993. Late Eocene–Recent volcanism and faulting in the southern main Ethiopian rift. Journal of the Geological Society 150 (1), 99–108.
Ferguson, D.J., Maclennan, J., Bastow, I.D., Pyle, D.M., Jones, S.M., Keir, D., Blundy, J. D., Plank, T., Yirgu, G., 2013. Melting during late-stage rifting in Afar is hot and deep. Nature 499 (7456), 70–73.
Field, L., Blundy, J., Calvert, A., Yirgu, G., 2013. Magmatic history of Dabbahu, a composite volcano in the Afar Rift, Ethiopia. Bulletin 125 (1–2), 128–147.
Fontijn, K., McNamara, K., Tadesse, A.Z., Pyle, D.M., Dessalegn, F., Hutchison, W., Mather, T.A., Yirgu, G., 2018. Contrasting styles of post-caldera volcanism along the Main Ethiopian Rift: Implications for contemporary volcanic hazards. Journal of Volcanology and Geothermal Research 356, 90–113.
Furman, T., Bryce, J., Rooney, T., Hanan, B., Yirgu, G., Ayalew, D., 2006. Heads and tails: 30 million years of the Afar plume. Geological Society, London, Special Publications 259 (1), 95–119.
Gasparon, M., Innocenti, F., Manetti, P., Peccerillo, A., Tsegaye, A., 1993. Genesis of the Pliocene to Recent bimodal mafic-felsic volcanism in the Debre Zeyt area, central Ethiopia: Volcanological and geochemical constraints. Journal of African Earth Sciences (and the Middle East) 17 (2), 145–165.
Giordano, F., D'Antonio, M., Civetta, L., Tonarini, S., Orsi, G., Ayalew, D., Yirgu, G., Dell'Erba, F., Di Vito, Isaia, R., 2014. Genesis and evolution of mafic and felsic magmas at Quaternary volcanoes within the Main Ethiopian Rift: Insights from Gedemsa and Fanta'Ale complexes. Lithos 188, 130–144.
Global Volcanism Program, 2013. Global Volcanism Program, Smithsonian Institution. Available at: https://volcano.si.edu/. Accessed: 10 October 2019.
Hammond, J.O., Kendall, J.M., Stuart, G.W., Keir, D., Ebinger, C., Ayele, A., Belachew, M., 2011. The nature of the crust beneath the Afar triple junction: Evidence from receiver functions. Geochemistry, Geophysics, Geosystems 12 (12).
Hofmann, C., Courtillot, V., Feraud, G., Rochette, P., Yirgu, G., Ketefo, E., Pik, R., 1997. Timing of the Ethiopian flood basalt event and implications for plume birth and global change. Nature 389 (6653), 838–841.
Hunt, J.A., Pyle, D.M., Mather, T.A., 2019. The geomorphology, structure, and lava flow dynamics of peralkaline rift volcanoes from high-resolution digital elevation models. Geochemistry, Geophysics, Geosystems 20 (3), 1508–1538.
Hutchison, W., Biggs, J., et al., 2016a. Causes of unrest at silicic calderas in the East African Rift: New constraints from InSAR and soil-gas chemistry at Aluto volcano, Ethiopia. Geochemistry, Geophysics, Geosystems 17 (8), 3008–3030. John Wiley & Sons, Ltd.
Hutchison, W., Pyle, D.M., et al., 2016b. The eruptive history and magmatic evolution of Aluto volcano: new insights into silicic peralkaline volcanism in the Ethiopian rift. Journal of Volcanology and Geothermal Research 328, 9–33. The Authors.
Hutchison, W., Mather, T.A., Pyle, D.M., Boyce, A.J., Gleeson, M.L., Yirgu, G., Blundy, J. D., Ferguson, D.J., Vye-Brown, C., Millar, I.L., Sims, K.W., 2018. The evolution of magma during continental rifting: New constraints from the isotopic and trace element signatures of silicic magmas from Ethiopian volcanoes. Earth and Planetary Science Letters 489, 203–218.
Irvine, T.N., Baragar, W.R.A., 1971. A guide to the chemical classification of the common volcanic rocks. Canadian journal of earth sciences 8 (5), 523–548.
Keir, D., Belachew, M., Ebinger, C.J., Kendall, J.M., Hammond, J.O., Stuart, G.W., Ayele, A., Rowland, J.V., 2011. Mapping the evolving strain field during continental breakup from crustal anisotropy in the Afar Depression. Nature Communications 2 (1), 285.
Klein, E.M., Langmuir, C.H., 1987. Global correlations of ocean ridge basalt chemistry with axial depth and crustal thickness. Journal of Geophysical Research: Solid Earth 92 (B8), 8089–8115.
Le Bas, M.J., Maitre, R.L., Streckeisen, A., Zanettin, B., 1986. A chemical classification of volcanic rocks based on the total alkali-silica diagram. Journal of petrology 27 (3), 745–750.
Leroy, S., d'Acremont, E., Tiberi, C., Basuyau, C., Autin, J., Lucazeau, F., Sloan, H., 2010. Recent off-axis volcanism in the eastern Gulf of Aden: implications for plume–ridge interaction. Earth and Planetary Science Letters 293 (1–2), 140–153.
Maguire, P.K.H., Keller, G.R., Klemperer, S.L., Mackenzie, G.D., Keranen, K., Harder, S., O'reilly, B., Thybo, H., Asfaw, L., Khan, M.A., Amha, M., 2006. Crustal structure of the northern Main Ethiopian Rift from the EAGLE controlled-source survey; a snapshot of incipient lithospheric break-up. Geological Society, London, Special Publications 259 (1), 269–292.
Mahood, G.A., 1984. Pyroclastic rocks and calderas associated with strongly peralkaline magmatism. Journal of Geophysical Research: Solid Earth 89 (10), 8540–8552.
Martí, J., Gudmundsson, A., 2000. The Las Cañadas caldera (Tenerife, Canary Islands): an overlapping collapse caldera generated by magma-chamber migration. Journal of volcanology and geothermal research 103 (1–4), 161–173.
McClusky, S., Reilinger, R., Ogubazghi, G., Amleson, A., Healeb, B., Vernant, P., Sholan, J., Fisseha, S., Asfaw, L., Bendick, R., Kogan, L., 2010. Kinematics of the southern Red Sea–Afar Triple Junction and implications for plate dynamics. Geophysical Research Letters 37 (5).
Mohr, P.A., Wood, C.A., 1976. Volcano spacings and lithospheric attenuation in the Eastern Rift of Africa. Earth and Planetary Science Letters 33 (1), 126–144.
Mohr, P., Mitchell, J.G., Raynolds, R.G.H., 1980. Quaternary volcanism and faulting at O'a Caldera. Central Ethiopian Rift. Bulletin Volcanologique 43, 173–189.
Niu, Y., 2021. Lithosphere thickness controls the extent of mantle melting, depth of melt extraction and basalt compositions in all tectonic settings on Earth–A review and new perspectives. Earth-Science Reviews 217, 103614.
Parnell-Turner, R., White, N., Henstock, T., Murton, B., Maclennan, J., Jones, S.M., 2014. A continuous 55-million-year record of transient mantle plume activity beneath Iceland. Nature Geoscience 7 (12), 914–919.
Patel, S., Solanki, P., 2020. Application of Landsat 8 OLI for Mapping the Deccan Traps of Kachchh Gujarat. Journal of the Indian Society of Remote Sensing 48, 1253–1263.
Peccerillo, A., Barberio, M.R., Yirgu, G., Ayalew, D., Barbieri, M.W.U.T.W., Wu, T.W., 2003. Relationships between mafic and peralkaline silicic magmatism in continental rift settings: a petrological, geochemical and isotopic study of the Gedemsa volcano, central Ethiopian rift. Journal of Petrology 44 (11), 2003–2032.
Pik, R., Deniel, C., Coulon, C., Yirgu, G., Hofmann, C., Ayalew, D., 1998. The northwestern Ethiopian Plateau flood basalts: classification and spatial distribution of magma types. Journal of Volcanology and Geothermal Research 81 (1–2), 91–111.
Putirka, K., Busby, C.J., 2007. The tectonic significance of high-K2O volcanism in the Sierra Nevada, California. Geology 35 (10), 923–926.
Ronga, F., Lustrino, M., Marzoli, A., Melluso, L., 2010. Petrogenesis of a basalt-comendite-pantellerite rock suite: the Boseti Volcanic Complex (Main Ethiopian Rift). Mineralogy and Petrology 98, 227–243.
Rooney, T.O., 2020a. The Cenozoic magmatism of East Africa: Part II – Rifting of the mobile belt. Lithos 360–361, 105291. Elsevier B.V.
Rooney, T.O., 2020b. 'The Cenozoic magmatism of East Africa: Part V – Magma sources and processes in the East African Rift. Lithos 360–361, 105296. Elsevier B.V.
Rooney, T.O., Furman, T., Yirgu, G., Ayalew, D., 2005. Structure of the Ethiopian lithosphere: Xenolith evidence in the Main Ethiopian Rift. Geochimica et Cosmochimica Acta 69 (15), 3889–3910.
Rooney, T., Furman, T., Bastow, I., Ayalew, D., Yirgu, G., 2007. Lithospheric modification during crustal extension in the Main Ethiopian Rift. Journal of Geophysical Research: Solid Earth 112 (B10).
Rooney, T.O., Hanan, B.B., et al., 2012a. Upper Mantle Pollution during Afar Plume–Continental Rift Interaction. Journal of Petrology 53 (2), 365–389. Oxford Academic.
Rooney, T.O., Hart, W.K., et al., 2012b. Peralkaline magma evolution and the tephra record in the Ethiopian Rift. Contributions to Mineralogy and Petrology 164 (3), 407–426. Springer Verlag.
Saria, E., Calais, E., Stamps, D.S., Delvaux, D., Hartnady, C.J.H., 2014. Present-day kinematics of the East African Rift. Journal of Geophysical Research: Solid Earth 119 (4), 3584–3600.
Siegburg, M., 2019. Evolution of Faulting and Magmatism during Volcanic Rifting in the Ethiopian Rift. (PhD Thesis). University of Southampton.
Siegburg, M., Gernon, T.M., Bull, J.M., Keir, D., Barfod, D.N., Taylor, R.N., Abebe, B., Ayele, A., 2018. Geological evolution of the Boset-Bericha volcanic complex, Main Ethiopian Rift: 40Ar/39Ar evidence for episodic Pleistocene to Holocene volcanism. Journal of Volcanology and Geothermal Research 351, 115–133.
Siegburg, M., Bull, J.M., Nixon, C.W., Keir, D., Gernon, T.M., Corti, G., Abebe, B., Sanderson, D.J., Ayele, A., 2020. Quantitative constraints on faulting and fault slip rates in the northern main Ethiopian Rift. Tectonics 39 (8) e2019TC006046.
Siegburg, M., Gernon, T.M., Keir, D., Bull, J.M., Taylor, R.N., Watts, E.J., Greenfield, T., Gebru, E.F., 2023. Temporal clustering of fissural eruption across multiple segments within the Ethiopian Rift. Frontiers in Earth Science 11, 1169635.
Stab, M., Bellahsen, N., Pik, R., Quidelleur, X., Ayalew, D., Leroy, S., 2016. Modes of rifting in magma-rich settings: Tectono-magmatic evolution of Central Afar. Tectonics 35 (1), 2–38.
Stewart, K., Rogers, N., 1996. Mantle plume and lithosphere contributions to basalts from southern Ethiopia. Earth and Planetary Science Letters 139 (1–2), 195–211.
Tesfaye, S., Harding, D.J., Kusky, T.M., 2003. Early continental breakup boundary and migration of the Afar triple junction, Ethiopia. Geological Society of America Bulletin 115 (9), 1053–1067.
Tortelli, G., Gioncada, A., Pagli, C., Braschi, E., Gebru, E.F., Keir, D., 2022. Constraints on the magma source and rift evolution from geochemistry of the Stratoid flood basalts (Afar, Ethiopia). Geochemistry, Geophysics, Geosystems 23 (8) e2022GC010434.
Trua, T., Deniel, C., Mazzuoli, R., 1999. Crustal control in the genesis of Plio-Quaternary bimodal magmatism of the Main Ethiopian Rift (MER): geochemical and isotopic (Sr, Nd, Pb) evidence. Chemical Geology 155 (3–4), 201–231.
Varet, J., 1975. Carte géologique de l'Afar central et méridional, 1:500 000. Géotechnip.
Varet, J., 2017. In: *Geology of Afar (East Africa)*. Springer.
Vidal, C.M., Fontijn, K., Lane, C.S., Asrat, A., Barfod, D., Tomlinson, E.L., Piermattei, A., Hutchison, W., Tadesse, A.Z., Yirgu, G., Deino, A., 2022. Geochronology and glass geochemistry of major pleistocene eruptions in the Main Ethiopian Rift: Towards a regional tephrostratigraphy. Quaternary Science Reviews 290, 107601.
Webster, J.D., Taylor, R.P., Bean, C., 1993. Pre-eruptive melt composition and constraints on degassing of a water-rich pantellerite magma, Fantale volcano, Ethiopia. Contributions to Mineralogy and Petrology 114, 53–62.
Williams, F.M., Williams, M.A.J., Aumento, F., 2004. Tensional fissures and crustal extension rates in the northern part of the Main Ethiopian Rift. Journal of African Earth Sciences 38 (2), 183–197.
Wolde, B., Widenfalk, L., 1994. Petrochemical and geochemical constraints on Cenozoic volcanism in Ethiopia. African Geosciences Reviews 1, 475–494.

Wolfenden, E., Ebinger, C., Yirgu, G., Deino, A., Ayalew, D., 2004. Evolution of the northern Main Ethiopian rift: birth of a triple junction. Earth and Planetary Science Letters 224 (1–2), 213–228.
Wolfenden, E., Ebinger, C., Yirgu, G., Renne, P.R., Kelley, S.P., 2005. Evolution of a volcanic rifted margin: Southern Red Sea, Ethiopia. Geological Society of America Bulletin 117 (7–8), 846–864.
Wong, K., Ferguson, D., Matthews, S., Morgan, D., Tadesse, A.Z., Sinetebeb, Y., Yirgu, G., 2022. Exploring rift geodynamics in Ethiopia through olivine-spinel Al-exchange thermometry and rare-earth element distributions. Earth and Planetary Science Letters 597, 117820.
Wright, T.J., Sigmundsson, F., Pagli, C., Belachew, M., Hamling, I.J., Brandsdóttir, B., Keir, D., Pedersen, R., Ayele, A., Ebinger, C., Einarsson, P., 2012. Geophysical constraints on the dynamics of spreading centres from rifting episodes on land. Nature Geoscience 5 (4), 242–250.
Zwaan, F., Corti, G., Sani, F., Keir, D., Muluneh, A.A., Illsley-Kemp, F., Papini, M., 2020. Structural analysis of the Western Afar Margin, East Africa: Evidence for multiphase rotational rifting. Tectonics 39 (7) e2019TC006043.